Chapter 1
Microscopic Cluster Models

P. Descouvemont and M. Dufour

Abstract We present an overview of microscopic cluster models, by focusing on the Resonating Group Method (RGM) and on the Generator Coordinate Method (GCM). The wave functions of a nuclear system are defined from cluster wave functions, with an exact account of antisymmetrization between all nucleons. For the sake of pedagogy, the formalism is mostly presented in simple conditions, i.e. we essentially assume spinless clusters, and single-channel calculations. Generalizations going beyond these limitations are outlined. We present the GCM in more detail, and show how to compute matrix elements between Slater determinants. Specific examples dealing with α+nucleus systems are presented. We also discuss some approximations of the RGM, and in particular, the renormalized RGM which has been recently developed. We show that the GCM can be complemented by the microscopic variant of the R-matrix method, which provides a microscopic description of unbound states. Finally, extensions of the GCM to multicluster and multichannel calculations are discussed, and illustrated by typical examples. In particular we compare different three-α descriptions of ^{12}C.

1.1 Introduction

Clustering is a well-known effect in light nuclei [1]. Historically, the observation of clustering started with the α particle, which presents a large binding energy and therefore tends to keep its own identity in light nuclei. A description of nuclear states

P. Descouvemont (✉)
Physique Nucléaire Théorique et Physique Mathématique, C.P. 229,
Université Libre de Bruxelles (ULB), 1050 Brussels, Belgium
e-mail: pdesc@ulb.ac.be

M. Dufour
IPHC Bat27, IN2P3-CNRS/Université de Strasbourg,
BP28, 67037 Strasbourg Cedex 2, France
e-mail: Marianne.Dufour@IReS.in2p3fr

C. Beck (ed.), *Clusters in Nuclei, Vol.2*, Lecture Notes in Physics 848,
DOI: 10.1007/978-3-642-24707-1_1,

based on a cluster structure was first suggested by Wheeler [2] and by Margenau [3], and then extended by Brink [4]. This formulation is known as the α-cluster model, and has been widely used in the literature (see for example Ref. [5]). A typical example of α cluster states is the second 0^+ level in ^{12}C, known as the Hoyle state [6], which presents a strong $\alpha + ^8$ Be cluster structure, and plays a crucial role in stellar evolution.

The cluster structure in α nuclei (i.e. with nucleon numbers $A=4n$) was clarified by Ikeda [7] who proposed a diagram which identifies situations where a cluster structure can be observed. The α model and its extensions were utilized by many authors to investigate the properties of α-particle nuclei such as ^{8}Be, ^{12}C, ^{16}O, etc. In particular, the interest for α-cluster models was recently revived by the hypothesis of a new form of nuclear matter, in analogy with the Bose–Einstein condensates [8].

If the α particle, owing to its large binding energy, plays a central role in clustering phenomena, it soon became clear that other cluster structures can be observed. Reviews of recent developments in cluster physics can be found in Refs. [9, 10]. In many nuclei, some states present an α +nucleus structure. A well known example is ^{7}Li, well described by an $\alpha + t$ model [11]. In recent years, clustering phenomena have been observed in several nuclei such as ^{16}O, ^{18}O, ^{19}F, etc. More exotic states were suggested by Freer et al. [12] who found evidence for an ^{6}He+^{6}He rotational band in ^{12}Be. This unusual structure was subsequently supported by various calculations (see, for example [13, 14]).

An important property of clustering is that it may change from level to level in the same nucleus [15]. There are many examples: in ^{5}He, the ground state present an $\alpha+n$ structure, whereas the $3/2^+$ excited state is better described by a t+d configuration [16]. More generally, many nuclei exhibit α-cluster bands in their high-energy region. Recently "extreme" α-clustering has been reported in the ^{18}O nucleus [17].

The observation of clustering effects is the basis of cluster models, which are essentially divided into two categories: (i) non-microscopic models, where the internal structure of the clusters is neglected [18, 19], and (ii) microscopic theories where the clusters are described by shell-model wave functions [20, 21]. The Schrödinger equation is written as

$$H\Psi = E_T\Psi, \tag{1.1.1}$$

where H is the Hamiltonian, $P\Psi$ the wave function, and E_T the total energy.

In non-microscopic approaches, the Hamiltonian of a system involving A nucleons distributed over N clusters is given by

$$H = \sum_{i=1}^{N} \frac{\mathbf{P}_i^2}{2M_i} + \sum_{i>j=1}^{N} V_{ij}(\mathbf{R}_i - \mathbf{R}_j), \tag{1.1.2}$$

where the N clusters with masses M_i have a space coordinate $\mathbf{R}_i$ and a momentum $\mathbf{P}_i$. In this definition, V_{ij} is a nucleus–nucleus interaction which can be local or non local. It may also depend on other cluster coordinates such as the spin or the velocity. Of course, the simplest variant is a two-cluster model ($N=2$) where, after

removal of the c.m. motion, the Hamiltonian only depends on the relative coordinate $\mathbf{r} = \mathbf{R}_1 - \mathbf{R}_2$. An important issue in non-microscopic models is the choice of the potentials V_{ij}. In general, these potentials are fitted on some properties of the system, such as binding energies or nucleus–nucleus phase shifts. In most cases they depend on the angular momentum between the clusters. It is well known that, to simulate the Pauli principle, this potential must satisfy some requirements. Deep potentials [19] or their supersymmetric partners [22] can partially account for antisymmetrization effects, although the associated wave functions neglect the structure of the clusters.

Non-microscopic theories can be extended to more than two clusters. For three-body models, the hyperspherical method [23] or the Faddeev approach [24] are efficient techniques. Because of their relative simplicity, at least for two-cluster variants, non-microscopic models can be directly extended to scattering states, i.e. to solutions of (1.1.2) at positive energies. This raises difficulties to properly include the asymptotic behaviour of the wave function, but is now well mastered for two-body and three-body scattering states.

The present work is devoted to microscopic cluster theories [20]. In a microscopic model, the Hamiltonian of the A-nucleon system is written as

$$H = \sum_{i=1}^{A} \frac{\mathbf{p}_i^2}{2m_N} + \sum_{i>j=1}^{A} v_{ij}(\mathbf{r}_i - \mathbf{r}_j), \tag{1.1.3}$$

where m_N is the nucleon mass (assumed to be equal for neutrons and protons), $\mathbf{r}_i$ and $\mathbf{p}_i$ are the space coordinate and momentum of nucleon i, and v_{ij} a nucleon–nucleon interaction. We explicitly mention the dependence on space coordinates, but v_{ij} may also depend on other nucleon coordinates. Until now, most microscopic cluster calculations neglect three-body forces (see however Ref. [25]).

Hamiltonian (1.1.3) is common to all microscopic theories, which explicitly treat all nucleons of the system. Examples are the shell model [26] and its "No-Core" extensions [27], the Antisymmetric Molecular Dynamics (AMD, see Ref. [28]), or the Fermionic Molecular Dynamics (FMD, see Ref. [29]). For small nucleon numbers (i.e. $A \leq 4$), efficient techniques are available to solve the Schrödinger equation with realistic nucleon–nucleon interactions (see Ref. [30] and references therein). These methods can be applied to bound as well as to continuum states. When the nucleon number is larger, some approximation must be used. The specificity of cluster models is that the wave function of the A-nucleon system, solution of the Schrödinger equation associated with (1.1.3), is described within the cluster approximation. In other words, the A nucleons are assumed to be divided in clusters, described by shell-model wave functions, and the total wave function is fully antisymmetric. For a two-cluster system with internal wave functions ϕ_1 and ϕ_2, the total wave function is written as

$$\Psi = \mathscr{A}\phi_1\phi_2 g(\boldsymbol{\rho}), \tag{1.1.4}$$

where $\mathscr{A}$ is the A-nucleon antisymmetrizor, and the radial function $g(\rho)$ depends on the relative coordinate $\boldsymbol{\rho}$. The cluster approximation is at the origin of the Resonating

Group Method (RGM) proposed by Wheeler [2] and widely used and developed by many groups (see for example [16, 20, 31]).

A significant breakthrough in microscopic cluster theories was achieved by the introduction of the Generator Coordinate Method (GCM), equivalent to the RGM, but allowing simpler and more systematic calculations [32]. The principle of the GCM is to expand the radial wave function $g(\boldsymbol{\rho})$ in a Gaussian basis. Under some restrictions, the total wave function (1.4) can then be rewritten as a combination of Slater determinants, well adapted to numerical calculations. Over the last decades, the GCM was developed in various directions: multi-cluster extensions [33–35], improved shell-model descriptions of the cluster wave functions [36], monopole distortion of the clusters [37], etc.

In nuclear spectroscopy, microscopic cluster models present a wide range of applications. They are remarkably well suited to molecular states, which are known to be strongly deformed, and present a marked cluster structure (see, for example, Refs. [13, 38–40]). The physics of exotic nuclei, and in particular of halo nuclei, is rather recent [41], and is also well described by cluster models. These nuclei are regarded as a core surrounded by external nucleons moving at large distances [42], and can be considered as cluster systems (see, for example, Refs. [43–45]). Unbound nuclei are extreme applications of cluster models, well adapted to resonances [46]. Several other applications, such as β decay [47] or charge symmetry in the Asymptotic Normalization Constant [48], have also been analyzed within microscopic cluster theories.

Microscopic cluster models have been also applied to various types of reactions: elastic, inelastic, transfer, etc. At low energies, the wavelength associated with the relative motion is large with respect to the typical dimensions of the system, and antisymmetrization effects are expected to be important. Microscopic theories have been widely applied in nuclear astrophysics (see e.g. [49, 50]), where measurements in laboratories are in general impossible at stellar energies [51–53]. This includes low-energy capture and transfer processes. Other nuclear reactions, such as nucleus–nucleus bremsstrahlung [54], have been studied in microscopic approaches. Being restricted to a limited number of cluster configurations (in general one), a microscopic cluster model is well adapted to the spectroscopy of low-lying states, and to low-energy reactions, where the level density and the number of open channels are limited.

It is of course impossible to provide an exhaustive bibliography of microscopic cluster theories. Excellent reviews can be found, for example, in Refs. [16, 20, 32, 55–57]. The paper is organized as follows. In Sect. 1.2, we discuss effective nucleon–nucleon interactions used in microscopic theories. In Sect. 1.3, we present the RGM in simple conditions: we consider systems made of two spinless clusters. We present an illustrative example with the $\alpha + n$ system. Section 1.4 is devoted to the GCM and to its link with the RGM. In Sect. 1.5 we give more specific information on the calculation of GCM matrix elements. In Sect. 1.6, we discuss some approximations and reformulations of the RGM equations. Section 1.7 is devoted to extensions of the model to multicluster and multichannel approaches. The treatment of scattering states in the GCM framework is outlined in Sect. 1.8. We discuss some applications of the RGM in Sect. 1.9. Concluding remarks are presented in Sect. 1.10.

1.2 Choice of the Nucleon–Nucleon Interaction

In the A-body Hamiltonian (1.1.3), the nucleon–nucleon interaction v_{ij} must account for the cluster approximation of the wave function. This leads to effective interactions, adapted to harmonic-oscillator orbitals. For example, using $0s$ orbitals for the α particle makes all matrix elements of non-central forces equal to zero. The effect of non-central components is simulated by an appropriate choice of the central effective interaction.

The nucleon–nucleon interaction contains Coulomb and nuclear terms and is written as

$$v_{ij}(r) = v_{ij}^{C}(r) + v_{ij}^{N}(r), \tag{1.2.1}$$

where the Coulomb term

$$v_{ij}^{C}(r) = \frac{e^2}{r}\left(\frac{1}{2} - t_{iz}\right)\left(\frac{1}{2} - t_{jz}\right), \tag{1.2.2}$$

is defined in the isospin formalism. For the nuclear term, most calculations performed with the RGM use central $v_{ij}^{N,c}(r)$ and spin–orbit $v_{ij}^{N,so}(r)$ interactions with

$$v_{ij}^{N}(r) = v_{ij}^{N,c}(r) + v_{ij}^{N,so}(r). \tag{1.2.3}$$

In general, the central part is written as a combination of N_g Gaussian form factors

$$v_{ij}^{N,c}(r) = \sum_{k=1}^{N_g} V_{0k}\exp(-(r/a_k)^2)(w_k - m_k P_{ij}^{\sigma} P_{ij}^{\tau} + b_k P_{ij}^{\sigma} - h_k P_{ij}^{\tau}). \tag{1.2.4}$$

Other potentials, such as the M3Y force [58] are defined from Yukawa form factors. However, the use of Gaussian form factors is well adapted to harmonic-oscillator orbitals. Parameters V_{0k} and a_k are given in Table 1.1 for the Volkov V2 [59] and Minnesota [60] interactions. Both forces contain one adjustable parameter (M and u, respectively). The standard values are $M=0.6$ and $u=1$, but these parameters can be slightly modified in order to reproduce an important property of the system. A typical example is the energy of a resonance or of a bound state.

The Volkov interaction involves two Gaussian functions and does not depend on spin and isospin ($b_k = h_k = 0$). With this force the deuteron binding energy is underestimated and the dineutron system is bound with the same energy. The Minnesota interaction [60] is defined by three different Gaussian functions. This force reproduces the deuteron binding energy and some properties of nucleon–nucleon scattering. It simulates the missing tensor force in the binding energy, as well as possible three-body effects, through the central term. Of course, the quadrupole moment of the deuteron, which is determined by the tensor force, is exactly zero with the Minnesota interaction.

Table 1.1 Amplitudes V_{0k} (in MeV) and ranges a_k (in fm) of the Volkov V2 and Minnesota interactions

Interaction	k	V_{0k}	a_k	w_k	m_k	b_k	h_k
Volkov V2	1	−60.65	1.80	$1-M$	M	0	0
	2	61.14	1.01	$1-M$	M	0	0
Minnesota	1	200	$1/\sqrt{1.487}$	$u/2$	$1-u/2$	0	0
	2	−178	$1/\sqrt{0.639}$	$u/4$	$1/2-u/4$	$u/4$	$1/2-u/4$
	3	−91.85	$1/\sqrt{0.465}$	$u/4$	$1/2-u/4$	$-u/4$	$u/4-1/2$

In Ref. [40], we have extended the Volkov *V*2 interaction by introducing Bartlett and Heisenberg components. This development was motivated by the need for more flexible interactions, able to reproduce thresholds in transfer reactions. This force is referred to as the EVI (Extended Volkov Interaction) interaction.

In most calculations a spin–orbit term is included. We take it as defined in Ref. [61] (see also [60]),

$$v_{ij}^{N,so}(\mathbf{r}) = -\frac{S_0}{\hbar^2 r_0^5}\big((\mathbf{r}_i-\mathbf{r}_j)\times(\mathbf{p}_i-\mathbf{p}_j)\big)\cdot(\mathbf{s}_i+\mathbf{s}_j)\exp\big(-(r/r_0)^2\big), \qquad (1.2.5)$$

where S_0 is the amplitude (expressed in MeV.fm^5), and $\mathbf{s}_i$ is the spin of nucleon i. Standard values of S_0 are $S_0 \approx 30$ MeV.fm^5, which provides a fair approximation of the $1/2^- - 3/2^-$ energy splitting in ^{15}N. We use a range $r_0 = 0.1$ fm, which is equivalent to a zero-range force.

As mentioned earlier, cluster models make use of effective nucleon–nucleon forces. In contrast, *ab initio* models [29, 62] aim at determining exact solutions of the Schrödinger equation (1.1.1), without the cluster approximation. For instance, the No-Core Shell Model (NCSM) is based on very large one-center harmonic-oscillator (HO) bases and effective interactions [63], derived from realistic forces such as Argonne [64] or CD-Bonn [65]. These interactions are adapted for finite model spaces through a particular unitary transformation. Wave functions are then expected to be accurate, but states presenting a strong clustering remain difficult to describe with this model. Indeed, in spite of considerable advances in computer facilities, the calculations remain limited by the size of the model space. Realistic interactions are adjusted to reproduce properties of the nucleon–nucleon system with a high precision. The necessity to introduce a 3*N* force or more (4*N*, ...) is now established in order to get highly accurate spectra [66]. However, genuine expressions of these potentials remain under study [66].

1.3 The Resonating Group Method

1.3.1 The RGM Equation

Let us consider A nucleons with coordinates $\mathbf{r}_i$, assumed to be divided in two clusters with A_1 and A_2 nucleons. The center of mass (c.m.) of each cluster is given by

$$\begin{aligned} \mathbf{R}_{cm,1} &= \frac{1}{A_1}\sum_{i=1}^{A_1}\mathbf{r}_i, \\ \mathbf{R}_{cm,2} &= \frac{1}{A_2}\sum_{i=A_1+1}^{A}\mathbf{r}_i, \end{aligned} \tag{1.3.1}$$

which define the c.m. of the system $\mathbf{R}_{cm}$, and the relative coordinate $\boldsymbol{\rho}$ as

$$\begin{aligned} \mathbf{R}_{cm} &= \frac{1}{A}\big(A_1\mathbf{R}_{cm,1} + A_2\mathbf{R}_{cm,2}\big), \\ \boldsymbol{\rho} &= \mathbf{R}_{cm,2} - \mathbf{R}_{cm,1}. \end{aligned} \tag{1.3.2}$$

For each cluster, we define a set of translation-invariant coordinates

$$\begin{aligned} \boldsymbol{\xi}_{1i} &= \mathbf{r}_i - \mathbf{R}_{cm,1} \quad \text{for } i = 1,\ldots,A_1, \\ \boldsymbol{\xi}_{2i} &= \mathbf{r}_i - \mathbf{R}_{cm,2} \quad \text{for } i = A_1+1,\ldots,A. \end{aligned} \tag{1.3.3}$$

The A_1 and A_2 sets of coordinates $\boldsymbol{\xi}_{1i}$ and $\boldsymbol{\xi}_{2i}$ are not independent since we have, according to the definitions of $\mathbf{R}_{cm,1}$ and $\mathbf{R}_{cm,2}$,

$$\sum_{i=1}^{A_1}\boldsymbol{\xi}_{1i} = \sum_{i=A_1+1}^{A}\boldsymbol{\xi}_{2i} = 0. \tag{1.3.4}$$

In the RGM, the total wave function is based on internal cluster wave functions $\phi_1(\boldsymbol{\xi}_{1i})$ and $\phi_2(\boldsymbol{\xi}_{2i})$. These internal wave functions are defined in the harmonic-oscillator model with oscillator parameter b. Here, we always assume that the oscillator parameter is common to all clusters. Going beyond this approximation introduces serious technical problems due to spurious c.m. components (see for example [16, 37, 67]). The RGM wave function is written, for two-cluster systems, as

$$\Psi(\boldsymbol{\xi}_{1i}, \boldsymbol{\xi}_{2i}, \boldsymbol{\rho}) = \mathscr{A}\phi_1(\boldsymbol{\xi}_{1i})\phi_2(\boldsymbol{\xi}_{2i})g(\boldsymbol{\rho}), \tag{1.3.5}$$

where $g(\boldsymbol{\rho})$ is the relative wave function, to be determined from the Schrödinger equation (1.1.1), and $\mathscr{A}$ the antisymmetrization operator

$$\mathscr{A} = \sum_{p=1}^{A!}\varepsilon_p P_p, \tag{1.3.6}$$

where P_p is a permutation over the A nucleons and $\varepsilon_p = \pm 1$ is the sign of this permutation. This operator not only acts inside the clusters, but also contains exchange terms between them. With this definition, the antisymmetrization operator is not exactly a projector since we have

$$\mathscr{A}^2 = A!\mathscr{A}. \tag{1.3.7}$$

In Eq. (1.3.5), we do not include the spins of the clusters, neither the relative angular momentum between the clusters. Definition (1.3.5) only contains one cluster configuration or, in other words, a single arrangement of the nucleons. More generally, several cluster wave functions (1.3.5) can be combined to improve the total wave function of the system. Here we limit ourselves to this simple case, for the sake of clarity. Various extensions will be developed in Sect. 1.7.

At first glance, the RGM wave function may appear as suitable for cluster states only, where the cluster approximation is obvious. However, owing to the antisymmetrization operator $\mathscr{A}$, the RGM (and the equivalent GCM described in Sect. 1.4) can be also applied to non-cluster states, such as shell-model or single-particle states [56].

Another remarkable advantage of the RGM wave function (1.3.5) is its direct applicability to scattering states. The main issue for scattering is to treat the asymptotic behaviour of the wave functions. At large relative distances between the colliding nuclei, antisymmetrization effects are negligible and the factorization (1.3.5) is exact without the antisymmetrization operator. This property is one of the main advantages of the RGM with respect to other microscopic approaches, such as the shell model or the FMD, where the treatment of scattering states is a serious problem, in particular to go beyond nucleon+nucleus scattering [68].

To derive the relative wave function $g(\rho)$, let us rewrite Eq. (1.3.5) as

$$\Psi = \mathscr{A}\phi_1\phi_2 g(\boldsymbol{\rho}) = \int \mathscr{A}\phi_1\phi_2\delta(\boldsymbol{\rho} - \mathbf{r})g(\mathbf{r})d\mathbf{r}, \tag{1.3.8}$$

where $\mathbf{r}$ is a parameter on which operator $\mathscr{A}$ does not act, and where the internal coordinates are implied. Then, using (1.3.8) in the Schrödinger equation (1.1.1) provides the RGM equation

$$\int \left[\mathscr{H}(\boldsymbol{\rho}, \boldsymbol{\rho}') - E_T\mathscr{N}(\boldsymbol{\rho}, \boldsymbol{\rho}')\right]g(\boldsymbol{\rho}')d\boldsymbol{\rho}' = 0. \tag{1.3.9}$$

In this equation, $\mathscr{N}$ and $\mathscr{H}$ are the (non-local) overlap and Hamiltonian kernels defined as

$$\left\{\begin{array}{c}\mathscr{N}(\boldsymbol{\rho}, \boldsymbol{\rho}')\\ \mathscr{H}(\boldsymbol{\rho}, \boldsymbol{\rho}')\end{array}\right\} = \langle\phi_1\phi_2\delta(\boldsymbol{\rho} - \mathbf{r})|\left\{\begin{array}{c}1\\ H\end{array}\right\}|\mathscr{A}\phi_1\phi_2\delta(\boldsymbol{\rho}' - \mathbf{r})\rangle, \tag{1.3.10}$$

where the integrals are performed over the internal coordinates and over the relative coordinate $\mathbf{r}$. In the Hamiltonian operator H, the kinetic energy of the center of mass (c.m.) has been subtracted. Accordingly E_T is defined with respect to the c.m. energy.

The RGM equation (1.3.9) can be simplified further by rewriting $\mathscr{A}$ and H as

$$\begin{aligned} \mathscr{A} &= 1 + \mathscr{A}' \\ H &= H_1 + H_2 + H', \end{aligned} \tag{1.3.11}$$

where $\mathscr{A}'$ only contains exchange terms, H_1 and H_2 are the internal Hamiltonians of the clusters, and H' is given by

$$H' = -\frac{\hbar^2}{2\mu}\Delta_\rho + \sum_{i=1}^{A_1}\sum_{j=A_1+1}^{A} v_{ij}, \tag{1.3.12}$$

μ being the reduced mass $\mu = \mu_0 m_N$ with $\mu_0 = A_1A_2/(A_1 + A_2)$. The internal energies E_1 and E_2 are given by

$$E_i = \langle \phi_i | H_i | \phi_i \rangle, \tag{1.3.13}$$

and the relative energy E is

$$E = E_T - E_1 - E_2. \tag{1.3.14}$$

In these conditions, kernels (1.3.10) can be expressed as

$$\begin{aligned} \mathscr{N}(\boldsymbol{\rho}, \boldsymbol{\rho}') &= \delta(\boldsymbol{\rho} - \boldsymbol{\rho}') + \mathscr{N}_E(\boldsymbol{\rho}, \boldsymbol{\rho}') \\ \mathscr{H}(\boldsymbol{\rho}, \boldsymbol{\rho}') &= \left(-\frac{\hbar^2}{2\mu}\Delta_\rho + V_D(\boldsymbol{\rho}) + E_1 + E_2\right)\delta(\boldsymbol{\rho} - \boldsymbol{\rho}') + \mathscr{H}_E(\boldsymbol{\rho}, \boldsymbol{\rho}') \end{aligned} \tag{1.3.15}$$

where $\mathscr{N}_E$ and $\mathscr{H}_E$ are the exchange kernels, and where the direct potential V_D is given by

$$V_D(\boldsymbol{\rho}) = \langle \phi_1\phi_2 | \sum_{i=1}^{A_1}\sum_{j=1}^{A_2} v_{ij} | \phi_1\phi_2 \rangle. \tag{1.3.16}$$

The RGM equation (1.3.9) is finally written as

$$\left(-\frac{\hbar^2}{2\mu}\Delta_\rho + V_D(\boldsymbol{\rho})\right) g(\boldsymbol{\rho}) + \int K(\boldsymbol{\rho}, \boldsymbol{\rho}') g(\boldsymbol{\rho}') d\boldsymbol{\rho}' = E g(\boldsymbol{\rho}), \tag{1.3.17}$$

with

$$K(\boldsymbol{\rho}, \boldsymbol{\rho}') = \mathscr{H}_E(\boldsymbol{\rho}, \boldsymbol{\rho}') - E_T \mathscr{N}_E(\boldsymbol{\rho}, \boldsymbol{\rho}'). \tag{1.3.18}$$

Equation (1.3.17) is the standard form of the RGM equation. It can be solved by different techniques (see for example [69]). The non-local term (1.3.18) is energy dependent and arises from exchange effects in the antisymmetrization operator (1.3.11). If $\mathscr{A}' = 0$, i.e. if antisymmetrization is neglected, the kernels $\mathscr{N}_E$ and $\mathscr{H}_E$ are equal to zero. In this simple approximation, the RGM equation is local and only involves the direct potential V_D.

1.3.2 Example: Overlap Kernel of the α+n System

This simple example illustrates the calculation of the overlap kernel. The extension to the Hamiltonian kernels is given in [70]. Let us consider the α and neutron internal wave functions

$$\begin{aligned} \phi_1 &= \Phi_\alpha(\boldsymbol{\xi}_1, \boldsymbol{\xi}_2, \boldsymbol{\xi}_3)|n_1 \downarrow n_1 \uparrow p_1 \downarrow p_1 \uparrow> \\ \phi_2 &= |n_2 \downarrow>, \end{aligned} \tag{1.3.19}$$

where we have factorized the space and spin/isospin components. The spatial component Φ_α of the α-particle wave function is built from $0s$ oscillator orbitals with parameter $\nu = 1/2b^2$. In the coordinate system (1.3.3) it is given as

$$\Phi_\alpha(\boldsymbol{\xi}_1, \boldsymbol{\xi}_2, \boldsymbol{\xi}_3) = \frac{1}{N}\exp(-\nu \sum_{i=1}^{4} \boldsymbol{\xi}_i^2), \tag{1.3.20}$$

with the normalization factor defined by

$$\begin{aligned} \langle \Phi_\alpha \mid \Phi_\alpha \rangle &= 1 \\ &= \frac{1}{N^2} \int\int\int \exp\left(-2\nu\left(\boldsymbol{\xi}_1^2+\boldsymbol{\xi}_2^2+\boldsymbol{\xi}_3^2 + (\boldsymbol{\xi}_1+\boldsymbol{\xi}_2+\boldsymbol{\xi}_3)^2\right)\right) d\boldsymbol{\xi}_1 d\boldsymbol{\xi}_2 d\boldsymbol{\xi}_3 \\ &= \frac{1}{N^2}\left(\frac{\pi^3}{32\nu^3}\right)^{3/2}. \end{aligned} \tag{1.3.21}$$

Notice that the internal wave function (1.3.20) only depends on three independent coordinates [see Eqs. (1.3.3, 1.3.4)]. Coordinate $\boldsymbol{\xi}_4$ is defined from (1.3.4).

Since we assume that the external neutron has a spin down, only the exchange operator P_{15} between nucleons 1 and 5 contributes in the antisymmetrization operator (1.3.6). Applying P_{15} on the internal and relative coordinates provides

$$\begin{aligned} P_{15}\boldsymbol{\xi}_1 &= \frac{3}{4}\boldsymbol{\rho} + \frac{1}{4}\boldsymbol{\xi}_1, \\ P_{15}\boldsymbol{\xi}_2 &= -\frac{1}{4}\boldsymbol{\rho} + \frac{1}{4}\boldsymbol{\xi}_1 + \boldsymbol{\xi}_2, \\ P_{15}\boldsymbol{\xi}_3 &= -\frac{1}{4}\boldsymbol{\rho} + \frac{1}{4}\boldsymbol{\xi}_1 + \boldsymbol{\xi}_3, \\ P_{15}\boldsymbol{\rho} &= -\frac{1}{4}\boldsymbol{\rho} + \frac{5}{4}\boldsymbol{\xi}_1. \end{aligned} \tag{1.3.22}$$

A simple calculation leads to

$$P_{15}\Phi_\alpha \delta(\boldsymbol{\rho} - \mathbf{r}) = \Phi_\alpha \exp\left[-\frac{4\nu}{5}\left(r^2 - (P_{15}\boldsymbol{\rho})^2\right)\right] \delta(P_{15}\boldsymbol{\rho} - \mathbf{r}), \tag{1.3.23}$$

and the exchange overlap kernel is deduced from (1.3.15) as

$$\mathcal{N}_E(\boldsymbol{\rho},\boldsymbol{\rho}') = -\int\int\int\int d\mathbf{r}d\boldsymbol{\xi}_1 d\boldsymbol{\xi}_2 d\boldsymbol{\xi}_3 \Phi_\alpha(\boldsymbol{\xi}_1,\boldsymbol{\xi}_2,\boldsymbol{\xi}_3) \times \delta(\boldsymbol{\rho}-\mathbf{r})P_{15}\Phi_\alpha(\boldsymbol{\xi}_1,\boldsymbol{\xi}_2,\boldsymbol{\xi}_3)\delta(\boldsymbol{\rho}'-\mathbf{r}). \tag{1.3.24}$$

The integral is first performed over $\mathbf{r}$. Then, integration over $\boldsymbol{\xi}_2$ and $\boldsymbol{\xi}_3$ provides

$$\int |\Phi_\alpha(\boldsymbol{\xi}_1,\boldsymbol{\xi}_2,\boldsymbol{\xi}_3)|^2 d\boldsymbol{\xi}_2 d\boldsymbol{\xi}_3 = \left(\frac{\sqrt{3}\pi}{6\nu}\right)^3 \exp\left(-\frac{8\nu}{3}\boldsymbol{\xi}_1^2\right). \tag{1.3.25}$$

This gives, by integrating over $\boldsymbol{\xi}_1$ and using the delta function in (1.3.23),

$$\mathcal{N}_E(\boldsymbol{\rho},\boldsymbol{\rho}') = -\left(\frac{4}{5}\right)^3 \left(\frac{8\nu}{3\pi}\right)^{3/2} \exp\left[-\frac{4\nu}{75}(17\boldsymbol{\rho}^2 + 17\boldsymbol{\rho}'^2 + 16\boldsymbol{\rho}\cdot\boldsymbol{\rho}')\right]. \tag{1.3.26}$$

This result can be also found in Refs. [70, 71] for example (see also Ref. [72]). Of course it does not depend on the spin and isospin of the external nucleon.

1.4 The Generator Coordinate Method

1.4.1 Introduction

The main problem associated with the RGM is not to solve the integro-differential equation (1.3.17). This can be done, for example, by using finite-difference methods [73], or the Lagrange-mesh technique [69, 74]. In contrast, the determination of the overlap and Hamiltonian kernels (1.3.10) requires heavy analytical calculations, in particular for systems involving *p*-shell clusters. The non-systematic character of the RGM makes it quite difficult to apply in multicluster systems or in multichannel problems.

This limitation received an efficient solution with the introduction of the Generator Coordinate Method [16, 32, 75]. The idea underlying the GCM is to expand the radial function $g(\boldsymbol{\rho})$ (1.3.5) over Gaussian functions, centered at different locations, called the generator coordinates. This expansion allows to express the total wave function (1.3.5) as a superposition of Slater determinants. The RGM and the GCM methods are therefore equivalent, but the use of Slater determinants makes the GCM better adapted to numerical calculations. The GCM has been applied, in the last decades, to many nuclei or reactions. In particular the spectroscopy of exotic nuclei [45, 76], and reactions of astrophysical interest [77] have been investigated.

1.4.2 Slater Determinants and GCM Basis Functions

Let us consider a one-center Slater determinant $\Phi_1(\mathbf{S})$ built from A_1 orbitals. All orbitals are centered at a common location $\mathbf{S}$ as

$$\Phi_1(\mathbf{S}) = \frac{1}{\sqrt{A_1!}} \det\left\{\hat{\varphi}_1(\mathbf{S}) \dots \hat{\varphi}_{A_1}(\mathbf{S})\right\} = \frac{1}{\sqrt{A_1!}} \mathscr{A}\hat{\varphi}_1(\mathbf{S}) \dots \hat{\varphi}_{A_1}(\mathbf{S}), \tag{1.4.1}$$

where the individual orbitals $\hat{\varphi}_i(\mathbf{S})$ are factorized in space, spin and isospin components. Each function $\hat{\varphi}_i(\mathbf{S})$ is therefore defined as

$$\hat{\varphi}_i(\mathbf{S}) = \varphi_i(\mathbf{r}, \mathbf{S})|m_{s_i}\rangle|m_{t_i}\rangle, \tag{1.4.2}$$

where $|m_{s_i}\rangle$ is a spinor and $|m_{t_i}\rangle$ the isospin function. In this definition, the space, spin and isospin coordinates are implied. The radial part $\varphi_i(\mathbf{r}, \mathbf{S})$ is an harmonic-oscillator function, normalized to unity [78]. For s waves, it reads

$$\varphi_i(\mathbf{r}, \mathbf{S}) = \varphi_{0s}(\mathbf{r}, \mathbf{S}) = (\pi b^2)^{-3/4} \exp\left(-\frac{(\mathbf{r} - \mathbf{S})^2}{2b^2}\right). \tag{1.4.3}$$

The parameter ν and oscillator energy $\hbar\omega$ are related to the oscillator parameter b as

$$\begin{aligned} \nu &= 1/2b^2 \\ \hbar\omega &= \frac{\hbar^2}{m_N b^2}. \end{aligned} \tag{1.4.4}$$

For p waves, the radial functions are

$$\varphi_i(\mathbf{r}, \mathbf{S}) = \varphi_{1p\mu}(\mathbf{r}, \mathbf{S}) = \frac{\sqrt{2}}{b}(\mathbf{r}_\mu - \mathbf{S}_\mu)\varphi_{0s}(\mathbf{r}, \mathbf{S}), \tag{1.4.5}$$

where index μ corresponds to the Cartesian coordinates (x,y,z). In the following we do not explicitly write the labels $0s$ or $1p\mu$ to the nucleon orbitals. We assume that all orbitals have a common oscillator parameter and are all centered at the same location. This is different from the AMD or FMD, where the oscillator parameters are optimized individually for each nucleon.

A drawback of the internal wave function (1.4.1) is that it is not invariant under translation. However, the Slater determinant (1.4.1) can be rewritten as

$$\Phi_1(\mathbf{S}) = \exp\left(-\frac{A_1}{2b^2}(\mathbf{R}_{cm,1} - \mathbf{S})^2\right)\phi_1, \tag{1.4.6}$$

where ϕ_1 is the translation-invariant function defined in Sect. 1.3.1, and where $\mathbf{R}_{cm,1}$ is the c.m. coordinate (1.3.1) of the system. The factorization (1.4.6) is known as the Bethe and Rose theorem [79], and assumes that all shells below some maximum are included in the Slater determinant (1.4.1).

Let us now consider a two-center wave function defined from two cluster functions (1.4.1) located at $\mathbf{S}_1$ and $\mathbf{S}_2$. The generator coordinate is defined as $\mathbf{R} = \mathbf{S}_2 - \mathbf{S}_1$. We choose the origin of the system along the axis between $\mathbf{S}_1$ and $\mathbf{S}_2$. The location of the origin is therefore defined by a parameter λ (with $0 \leq \lambda \leq 1$). Typical values are $\lambda = 0$ which corresponds to the center of cluster 1, and $\lambda = A_2/A$, where the origin is located at the center of mass. We define the two-cluster Slater determinant as

$$\begin{aligned}\Phi(\mathbf{R}) &= \frac{1}{\sqrt{A!}} \det\left\{\hat{\varphi}(-\lambda\mathbf{R}) \ldots \hat{\varphi}_{A_1}(-\lambda\mathbf{R})\hat{\varphi}_{A_1+1}((1-\lambda)\mathbf{R}) \ldots \hat{\varphi}_A((1-\lambda)\mathbf{R})\right\}, \\ &= \frac{1}{\sqrt{N_0}} \mathscr{A}\Phi_1(-\lambda\mathbf{R})\Phi_2((1-\lambda)\mathbf{R}), \end{aligned} \tag{1.4.7}$$

where the nucleon coordinates are implied. The normalization factor $N_0 = \frac{A!}{A_1!A_2!}$ stems from property (1.3.7). This Slater determinant is built with A_1 orbitals at $-\lambda\mathbf{R}$ and A_2 orbitals at $(1-\lambda)\mathbf{R}$. Definition (1.4.7) can be directly extended to more than two clusters [21, 32, 80]. Obviously this basis function is not invariant under translation. However, by using the factorization (1.4.6) for both clusters, and assuming a common oscillator parameter b, Eq. (1.4.7) can be rewritten as

$$\Phi(\mathbf{R}) = \frac{1}{\sqrt{N_0}} \Phi_{cm}\mathscr{A}\phi_1\phi_2\Gamma(\boldsymbol{\rho}, \mathbf{R}), \tag{1.4.8}$$

which involves the translation-invariant functions ϕ_1 and ϕ_2. The c.m. and radial wave functions read

$$\begin{aligned}\Phi_{cm}(\mathbf{R_{cm}}) &= \left(\frac{A}{\pi b^2}\right)^{3/4} \exp\left(-\frac{A}{2b^2}\left[\mathbf{R}_{cm} + \mathbf{R}(\lambda - A_2/A)\right]^2\right), \\ \Gamma(\boldsymbol{\rho}, \mathbf{R}) &= \left(\frac{\mu_0}{\pi b^2}\right)^{3/4} \exp\left(-\frac{\mu_0}{2b^2}(\boldsymbol{\rho} - \mathbf{R})^2\right). \end{aligned} \tag{1.4.9}$$

The c.m. and radial coordinates are therefore uncoupled. The associated functions are simple Gaussian functions with oscillator parameters $b/\sqrt{A}$ and $b/\sqrt{\mu_0}$, respectively. This factorization of the c.m. motion greatly simplifies the calculation of GCM matrix elements. Let us express the Slater determinant (1.4.7) as

$$\Phi(\mathbf{R}) = \Phi_{cm}\bar{\Phi}(\mathbf{R}), \tag{1.4.10}$$

where $\bar{\Phi}(\mathbf{R})$ is a physical basis function, independent of the c.m. coordinate. Functions $\Phi(\mathbf{R})$, on the contrary, contain spurious c.m. components, but are well adapted to a numerical calculation since they are Slater determinants. Using (1.4.10), we have

$$\langle\Phi(\mathbf{R})|\Phi(\mathbf{R}')\rangle = \langle\Phi_{cm}|\Phi_{cm}\rangle\langle\bar{\Phi}(\mathbf{R})|\bar{\Phi}(\mathbf{R}')\rangle, \tag{1.4.11}$$

with

$$\langle \Phi_{cm} | \Phi_{cm} \rangle = \exp\left(-\frac{A(\lambda - A_2/A)^2}{4b^2} (\mathbf{R} - \mathbf{R}')^2 \right). \tag{1.4.12}$$

The overlap between basis functions $\bar{\Phi}(\mathbf{R})$ is therefore obtained from a matrix elements between Slater determinants, corrected by a simple c.m. factor. Notice that both c.m. functions in the matrix elements (1.4.12) may involve different generator coordinates.

Matrix elements between GCM basis states $\bar{\Phi}(\mathbf{R})$ should not depend on λ. This provides a strong test of the calculations. The choice $\lambda = A_2/A$, i.e. taking the origin at the center of mass, is commonly used since c.m. correction factors are trivial. Another choice adopted in the literature is $\lambda = 0$, where all orbitals are centred at the origin of cluster 1. If the orbitals of the external clusters are orthogonalized to the core orbitals [32, 81], the calculation of matrix elements is strongly simplified (see Sect. 1.5). This technique is quite efficient when the core is a closed-shell nucleus (α, ^{16}O, ^{40}Ca, etc.) and is surrounded by 0s orbitals (see for example Ref. [82] for the ^{16}O+^{3}He+p three-cluster system).

Matrix elements of other operators should account for the spurious c.m. contribution. Garthenaus and Schwartz [83] have shown that the removal of the c.m. component of the wave function can be achieved by using transformed operators, obtained by a modification of the space and momentum coordinates as

$$\begin{aligned} \mathbf{r}_i &\longrightarrow \mathbf{r}_i - \mathbf{R}_{cm} \\ \mathbf{p}_i &\longrightarrow \mathbf{p}_i - \frac{1}{A}\mathbf{P}_{cm}, \end{aligned} \tag{1.4.13}$$

where $\mathbf{P}_{cm}$ is the c.m. momentum. The transformation-invariant forms of the kinetic energy and of the r.m.s. radius are therefore

$$\begin{aligned} T &\longrightarrow T - T_{cm} = \sum_i \frac{\mathbf{p}_i^2}{2m_N} - T_{cm}, \\ < r^2 > &\longrightarrow < r^2 > - \mathbf{R}_{cm}^2 = \frac{1}{A}\sum_i \mathbf{r}_i^2 - \mathbf{R}_{cm}^2, \end{aligned} \tag{1.4.14}$$

and the c.m. matrix elements take the simple forms

$$\begin{aligned} \langle \Phi_{cm} | T_{cm} | \Phi_{cm} \rangle &= \frac{1}{4}\hbar\omega \left(3 - \frac{A(\lambda - A_2/A)^2}{2b^2} (\mathbf{R} - \mathbf{R}')^2 \right) \langle \Phi_{cm} | \Phi_{cm} \rangle \\ \langle \Phi_{cm} \left| \mathbf{R}_{cm}^2 \right| \Phi_{cm} \rangle &= \left(\frac{3}{2}b^2 + \frac{(\lambda - A_2/A)^2}{4} (\mathbf{R} + \mathbf{R}')^2 \right) \langle \Phi_{cm} | \Phi_{cm} \rangle. \end{aligned} \tag{1.4.15}$$

A similar calculation can be performed for the electric operators of rank L [84]. At the long-wavelength approximation, the translation-invariant form is defined as

$$\mathscr{M}^E_{LM} = e \sum_i \left(\frac{1}{2} - t_{iz} \right) |\mathbf{r}_i - \mathbf{R}_{cm}|^L Y^M_L(\Omega_{\mathbf{r}_i - \mathbf{R}_{cm}}). \tag{1.4.16}$$

This operator can be expanded as [78]

$$\mathscr{M}^E_{LM} = \sum_k \left(\frac{4\pi(2L+1)!}{(2k+1)!(2L-2k+1)!} \right)^{1/2} \left[\mathscr{M}^E_{L-k}(\mathbf{r}_i) \otimes \mathscr{M}^E_k(\mathbf{R}_{cm}) \right]^{LM}, \tag{1.4.17}$$

where $\mathscr{M}^E_{L-k}(\mathbf{r}_i)$ is defined from (1.4.16) and where the c.m. contributions read

$$\mathscr{M}^E_{km}(\mathbf{R}_{cm}) = R^k_{cm} Y^m_k(\Omega_{\mathbf{R}_{cm}}). \tag{1.4.18}$$

Matrix elements can be obtained as in (1.4.15). However, the calculation of additional multipoles ($k < L$) can be avoided by choosing $\lambda = A_2/A$ or, in other words, by taking the c.m. as origin of the coordinate system. In that case, only k=0 contributes in the matrix elements of (1.4.17) and the c.m. correction is trivial. Similar developments can be performed for magnetic multipoles [85].

The factorization of the internal wave functions and of the radial part makes GCM basis functions (1.4.8) well adapted to collisions (see Sect. 1.8). If the oscillator parameters of the clusters are different, the removal of the spurious c.m. components is however a delicate problem [16, 86]. This can be tackled by using the Complex GCM [16]. In this variant the generator coordinate $\mathbf{R}$ is complex. The calculation of matrix elements is very similar, but the imaginary part provides an efficient tool to deal with different oscillator parameters of the clusters.

1.4.3 Equivalence Between RGM and GCM

In the two-cluster approximation, the total wave function of a system is defined as a superposition of GCM basis functions

$$\Psi = \Phi^{-1}_{cm} \int f(\mathbf{R}) \Phi(\mathbf{R}) d\mathbf{R}, \tag{1.4.19}$$

where $f(\mathbf{R})$ is the generator function, to be determined from the microscopic Hamiltonian (1.1.3) According to Eq. (1.4.8), wave function Ψ is invariant under translation. Using (1.4.8), wave function (1.4.19) reads

$$\Psi = \mathscr{A} \phi_1 \phi_2 g(\boldsymbol{\rho}), \tag{1.4.20}$$

with

$$g(\boldsymbol{\rho}) = \int f(\mathbf{R}) \Gamma(\boldsymbol{\rho}, \mathbf{R}) d\mathbf{R}, \tag{1.4.21}$$

which shows the equivalent between the RGM and the GCM. The generator function is obtained from the Hill–Wheeler equation [87]

$$\int \left[H(\mathbf{R},\mathbf{R}') - E_T N(\mathbf{R},\mathbf{R}')\right] f(\mathbf{R}') d\mathbf{R}' = 0, \tag{1.4.22}$$

where the GCM kernels are given by

$$\left\{ \begin{array}{c} N(\mathbf{R},\mathbf{R}') \\ H(\mathbf{R},\mathbf{R}') \end{array} \right\} = \langle \bar{\Phi}(\mathbf{R})| \left\{ \begin{array}{c} 1 \\ H \end{array} \right\} |\bar{\Phi}(\mathbf{R}')\rangle, \tag{1.4.23}$$

and where c.m. components have been removed. In practice the integral in (1.4.21) is discretized over a finite set of R_n values as

$$g(\boldsymbol{\rho}) \approx \sum_n f(\mathbf{R}_n) \Gamma(\boldsymbol{\rho}, \mathbf{R}_n). \tag{1.4.24}$$

For bound states, the integral equation (1.4.22) is therefore replaced by the diagonalization of a matrix (typically 10 R_n values are used). The treatment of scattering states requires an additional tool to correct for the Gaussian asymptotic behaviour of the relative function (1.4.24). This will be developed in Sect. 1.8.

The calculation of matrix elements between Slater determinants is well known [4] and will be discussed in Sect. 1.5 (see also Refs. [32, 67] for further detail). The RGM and GCM kernels [(1.3.10) and (1.4.23), respectively] can be linked to each other by integral transforms [32, 67, 88].

1.4.4 Two-Cluster Angular-Momentum Projection

Let us consider the partial-wave expansion of the GCM basis states (1.4.7)

$$\Phi(\mathbf{R}) = 4\pi \sum_{\ell m} \Phi^{\ell m}(R) Y_\ell^{m*}(\Omega_R). \tag{1.4.25}$$

Notice that the overall normalization does not play a role, and can be chosen freely as long as it is consistently used in the calculation of the matrix elements. We use the expansion of (1.4.9)

$$\begin{aligned} \Gamma(\boldsymbol{\rho},\mathbf{R}) &= 4\pi \sum_{\ell m} \Gamma_\ell(\rho,R) Y_\ell^m(\Omega_\rho) Y_\ell^{m*}(\Omega_R), \\ \Gamma_\ell(\rho,R) &= \left(\frac{\mu_0}{\pi b^2}\right)^{3/4} \exp\left[-\frac{\mu_0}{2b^2}(\rho^2+R^2)\right] i_\ell\left(\frac{\mu_0 \rho R}{b^2}\right), \end{aligned} \tag{1.4.26}$$

where $i_\ell(x)$ is a spherical Bessel function [89]. Then Eqs. (1.4.8) and (1.4.25) provide

$$\Phi^{\ell m}(R) = \frac{1}{\sqrt{N_0}} \mathscr{A} \phi_1 \phi_2 \Gamma_\ell(\rho,R) Y_\ell^m(\Omega_\rho) \tag{1.4.27}$$

and the total wave function reads

$$\Psi^{\ell m} = \int f_\ell(R)\Phi^{\ell m}(R)dR. \tag{1.4.28}$$

The generator function $f_\ell(R)$ is obtained from the Hill–Wheeler equation involving projected GCM kernels

$$\int \left[H_\ell(R,R') - E_T N_\ell(R,R')\right] f_\ell(R')dR' = 0. \tag{1.4.29}$$

The projected overlap kernel $N_\ell(R,R')$ is derived from the expansion

$$\begin{aligned} N(\mathbf{R},\mathbf{R}') &= \langle \Phi(\mathbf{R})|\Phi(\mathbf{R}')\rangle \\ &= (4\pi)^2 \sum_{\ell m} \langle \Phi_\ell(R)|\Phi_\ell(R')\rangle Y_\ell^m(\Omega_R) Y_\ell^{m*}(\Omega_{R'}) \\ &= 4\pi \sum_\ell (2\ell+1)\langle \Phi_\ell(R)|\Phi_\ell(R')\rangle P_\ell(\cos\theta), \end{aligned} \tag{1.4.30}$$

where θ is the angle between $\mathbf{R}$ and $\mathbf{R}'$. Then, by inverting (1.4.30), we find

$$N_\ell(R,R') = \langle \Phi_\ell(R)|\Phi_\ell(R')\rangle = \frac{1}{8\pi}\int_0^\pi N(\mathbf{R},\mathbf{R}')P_\ell(\cos\theta)d\cos\theta, \tag{1.4.31}$$

and a similar equation holds for the Hamiltonian kernel $H_\ell(R,R')$. Since $N(\mathbf{R},\mathbf{R}')$ and $H(\mathbf{R},\mathbf{R}')$ only depend on the relative angle θ, the orientation of one generator coordinate can be chosen arbitrarily. A common choice is to take $\mathbf{R}$ along the z axis, and $\mathbf{R}'$ in the xz plane. The integration over θ can be performed numerically with a Gauss–Legendre quadrature, or analytically in some simple cases.

For two-clusters systems, the projection over parity is automatic since the angular-momentum projection provides

$$\pi = (-1)^\ell. \tag{1.4.32}$$

1.5 Matrix Elements Between Slater Determinants

1.5.1 General Presentation

Let us consider a system of A orbitals $\hat{\varphi}_i(\mathbf{S}_n)$ distributed among N clusters. The set of cluster locations is denoted as $\mathbf{S}_{\{N\}}$. As mentioned in (1.4.2) the individual orbitals involve space, spin and isospin components as

$$\hat{\varphi}_i(\mathbf{S}_n) = |\varphi_i(\mathbf{r},\mathbf{S}_n)\rangle |m_{s_i}\rangle |m_{t_i}\rangle, \tag{1.5.1}$$

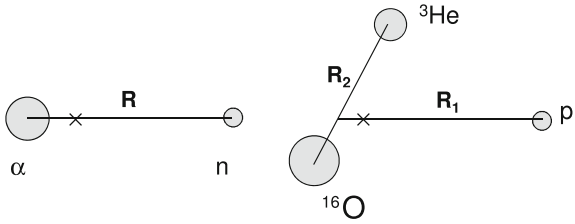

Fig. 1.1 Typical two-cluster ($\alpha + \mathrm{n}$) and three-cluster ($^{16}\mathrm{O}+^{3}\mathrm{He}+\mathrm{p}$) configurations. The crosses indicate the c.m. location within the generator coordinates

where $\varphi_i(\mathbf{r}, \mathbf{S}_n)$ is an harmonic-oscillator function. Most calculations are performed with $0s$ orbitals, but the presentation is more general; explicit definitions of s and p orbitals are given by (1.4.3) and (1.4.5). The A-nucleon Slater determinant reads

$$\Phi(\mathbf{S}_{\{N\}}) = \frac{1}{\sqrt{A!}} \det\{\hat{\varphi}_1(\mathbf{S}_1) \dots \hat{\varphi}_A(\mathbf{S}_N)\}. \tag{1.5.2}$$

For example, the $\alpha + \mathrm{n}$ system involves four s orbitals at $\mathbf{S}_1 = -\mathbf{R}/5$, and one $0s$ orbital at $\mathbf{S}_2 = 4\mathbf{R}/5$. The ^{19}Ne+p system, with ^{19}Ne described as $^{16}\mathrm{O}+^{3}\mathrm{He}$ [82], involves four $0s$ and twelve $1p$ orbitals at $\mathbf{S}_1 = -\mathbf{R}_1/20 - 3\mathbf{R}_2/19$, three $0s$ orbitals at $\mathbf{S}_2 = -\mathbf{R}_1/20 + 16\mathbf{R}_2/19$, and one $0s$ orbital at $\mathbf{S}_3 = 19\mathbf{R}_1/20$ (see Fig. 1.1).

The calculation of matrix elements between Slater determinants (1.5.2) is rather simple and systematic. We present here a short overview of the method, but more detail can be found in Refs. [4, 32]. The overlap is given by

$$\begin{aligned}
\langle \Phi(\mathbf{S}_{\{N\}}) | \Phi(\mathbf{S}'_{\{N\}}) \rangle &= \frac{1}{A!} \langle \mathscr{A}\hat{\varphi}_1(\mathbf{S}_1) \dots \hat{\varphi}_A(\mathbf{S}_N) \mid \mathscr{A}\hat{\varphi}_1(\mathbf{S}'_1) \dots \hat{\varphi}_A(\mathbf{S}'_N) \rangle \\
&= \langle \hat{\varphi}_1(\mathbf{S}_1) \dots \hat{\varphi}_A(\mathbf{S}_N) \mid \mathscr{A}\hat{\varphi}_1(\mathbf{S}'_1) \dots \hat{\varphi}_A(\mathbf{S}'_N) \rangle \\
&= \langle \hat{\varphi}_1(\mathbf{S}_1) \dots \hat{\varphi}_A(\mathbf{S}_N) \mid \det \hat{\varphi}_1(\mathbf{S}'_1) \dots \hat{\varphi}_A(\mathbf{S}'_N) \rangle \\
&= \det \mathbf{B},
\end{aligned} \tag{1.5.3}$$

where we have used (1.3.7), and where matrix $\mathbf{B}$ is given by the individual overlaps as

$$B_{ij} = \langle \hat{\varphi}_i(\mathbf{S}_i) | \hat{\varphi}_j(\mathbf{S}'_j) \rangle. \tag{1.5.4}$$

For one-body operators O_1 written as

$$O_1 = \sum_{i=1}^{A} o_1(\mathbf{r}_i), \tag{1.5.5}$$

a matrix element between Slater determinants reads

$$\begin{aligned}\langle O_1\rangle &= \langle \Phi(\mathbf{S}_{\{N\}})|O_1|\Phi(\mathbf{S}'_{\{N\}})\rangle \\ &= \sum_{ij=1}^{A} M_{ij}\langle\hat{\varphi}_i(\mathbf{S}_i)|o_1|\hat{\varphi}_j(\mathbf{S}'_j)\rangle \\ &= \det\mathbf{B}\sum_{ij=1}^{A}\left(\mathbf{B}^{-1}\right)_{ji}\langle\hat{\varphi}_i(\mathbf{S}_i)|o_1|\hat{\varphi}_j(\mathbf{S}'_j)\rangle \quad \text{if } \det\mathbf{B}\neq 0, \end{aligned} \tag{1.5.6}$$

where M_{ij} is a cofactor of matrix $\mathbf{B}$. It is obtained from the determinant of $\mathbf{B}$ after removal of column i and line j, and multiplication by a phase factor $(-1)^{i+j}$. If $\det\mathbf{B}\neq 0$, we have

$$M_{ij} = \det\mathbf{B}\left(\mathbf{B}^{-1}\right)_{ji}. \tag{1.5.7}$$

One-body matrix elements therefore involve a double sum over the individual orbitals. Here and in the following, we assume $\det\mathbf{B}\neq 0$, but the generalization is straightforward. Typical examples of one-body operators are the kinetic energy, the r.m.s. radius, and the electromagnetic operators.

For a two-body operators O_2 such as the nucleon–nucleon interaction

$$O_2 = \sum_{i>j=1}^{A} o_2(\mathbf{r}_i,\mathbf{r}_j) = \frac{1}{2}\sum_{i\neq j=1}^{A} o_2(\mathbf{r}_i,\mathbf{r}_j), \tag{1.5.8}$$

a matrix element reads

$$\begin{aligned}\langle O_2\rangle &= \langle \Phi(\mathbf{S}_{\{N\}})|O_2|\Phi(\mathbf{S}'_{\{N\}})\rangle \\ &= \frac{1}{2}\sum_{ijkl=1}^{A} M_{ij,kl}\langle\hat{\varphi}_i(\mathbf{S}_i)\hat{\varphi}_j(\mathbf{S}_j)|o_2|\hat{\varphi}_k(\mathbf{S}'_k)\hat{\varphi}_l(\mathbf{S}'_l)\rangle, \end{aligned} \tag{1.5.9}$$

where $M_{ij,kl}$ is a second-order cofactor of matrix $\mathbf{B}$. For $\det\mathbf{B}\neq 0$, we have

$$M_{ij,kl} = \det\mathbf{B}\left[\left(\mathbf{B}^{-1}\right)_{ki}\left(\mathbf{B}^{-1}\right)_{lj} - \left(\mathbf{B}^{-1}\right)_{kj}\left(\mathbf{B}^{-1}\right)_{li}\right]. \tag{1.5.10}$$

In addition since the individual matrix elements satisfy the symmetry property

$$\langle\varphi_i(\mathbf{S}_i)\varphi_j(\mathbf{S}_j)|o_2|\varphi_k(\mathbf{S}'_k)\varphi_l(\mathbf{S}'_l)\rangle = \langle\varphi_j(\mathbf{S}_j)\varphi_i(\mathbf{S}_i)|o_2|\varphi_l(\mathbf{S}'_l)\varphi_k(\mathbf{S}'_k)\rangle, \tag{1.5.11}$$

the following definitions are equivalent:

$$\begin{aligned}\langle O_2\rangle =&\frac{1}{2}\det\mathbf{B}\sum_{ijkl=1}^{A}\left[\left(\mathbf{B}^{-1}\right)_{ki}\left(\mathbf{B}^{-1}\right)_{lj}-\left(\mathbf{B}^{-1}\right)_{kj}\left(\mathbf{B}^{-1}\right)_{li}\right]\\ &\times\langle\hat{\varphi}_i(\mathbf{S}_i)\hat{\varphi}_j(\mathbf{S}_j)|o_2|\hat{\varphi}_k(\mathbf{S}'_k)\hat{\varphi}_l(\mathbf{S}'_l)\rangle\\ =&\frac{1}{2}\det\mathbf{B}\sum_{ijkl=1}^{A}\left(\mathbf{B}^{-1}\right)_{ki}\left(\mathbf{B}^{-1}\right)_{lj}\left[\langle\hat{\varphi}_i(\mathbf{S}_i)\hat{\varphi}_j(\mathbf{S}_j)|o_2|\hat{\varphi}_k(\mathbf{S}'_k)\hat{\varphi}_l(\mathbf{S}'_l)\rangle\right.\\ &\left.-\langle\hat{\varphi}_i(\mathbf{S}_i)\hat{\varphi}_j(\mathbf{S}_j)|o_2|\hat{\varphi}_l(\mathbf{S}'_l)\hat{\varphi}_k(\mathbf{S}'_k)\rangle\right]. \qquad (1.5.12)\end{aligned}$$

They involve a quadruple sum over the individual orbitals. In practice the two-body matrix elements represent the main part of the computer time. Further extensions to three-body forces can be done, but the corresponding matrix elements involve sextuple sums overs the individual orbitals.

1.5.2 Spin and Isospin Factorization

In Eq. (1.5.1) it is assumed that the individual orbitals are characterized by spin and isposin projections ($m_s = \pm 1/2, m_t = \pm 1/2$). In that case, the overlap matrix $\mathbf{B}$ takes the simpler form

$$\mathbf{B}=\begin{pmatrix}\mathbf{B}^{n\downarrow} & & & \\ & \mathbf{B}^{n\uparrow} & & \\ & & \mathbf{B}^{p\downarrow} & \\ & & & \mathbf{B}^{p\uparrow}\end{pmatrix}, \qquad (1.5.13)$$

involving (smaller) submatrices corresponding to the nucleon types. The individual orbitals have been reordered in four groups corresponding to the spin and isospin values (notice that a phase factor (-1) may appear in the wave function when reordering the orbitals). The overlap (1.5.3) is then factorized as

$$\begin{aligned}\det\mathbf{B}&=\prod_{k=1}^{4}\det\mathbf{B}^k,\\ B^k_{ij}&=\langle\varphi_i(\mathbf{S}_i)|\varphi_j(\mathbf{S}'_j)\rangle, \qquad (1.5.14)\end{aligned}$$

where only the spatial parts of the wave functions are involved [see Eq. (1.5.1)]. In this definition, index k corresponds to the four spin/isospin projections. This means that the calculation is much faster than by using the full matrix. In many cases some of the matrices $\mathbf{B}^k$ are identical (for example in $n\alpha$ systems such as ^{8}Be or ^{12}C, the four matrices $\mathbf{B}^k$ are identical), which still simplifies the calculations.

If the one-body operator O_1 does not depend on spin and isospin (as for the kinetic energy for example), its matrix element (1.5.6) is simplified to

Table 1.2 Direct and exchange coefficients ($k_1 \geq k_2$) for the nuclear (central), Coulomb and spin–orbit interactions

$k_1\, k_2$	$A_D^{k_1k_2}$				$C_D^{k_1k_2}$	$S_D^{k_1k_2}$	$A_E^{k_1k_2}$				$C_E^{k_1k_2}$	$S_E^{k_1k_2}$
	1	$P^\sigma P^\tau$	P^σ	P^τ			1	$P^\sigma P^\tau$	P^σ	P^τ		
$n\downarrow\, n\downarrow$	1	1	1	1	0	−1	1	1	1	1	0	−1
$n\downarrow\, n\uparrow$	1	0	0	1	0	0	0	1	1	0	0	0
$n\downarrow\, p\downarrow$	1	0	1	0	0	−1	0	1	0	1	0	0
$n\downarrow\, p\uparrow$	1	0	0	0	0	0	0	1	0	0	0	0
$n\uparrow\, n\uparrow$	1	1	1	1	0	1	1	1	1	1	0	1
$n\uparrow\, p\downarrow$	1	0	0	0	0	0	0	1	0	0	0	0
$n\uparrow\, p\uparrow$	1	0	1	0	0	1	0	1	0	1	0	0
$p\downarrow\, p\downarrow$	1	1	1	1	1	−1	1	1	1	1	1	−1
$p\downarrow\, p\uparrow$	1	0	0	1	1	0	0	1	1	0	0	0
$p\uparrow\, p\uparrow$	1	1	1	1	1	1	1	1	1	1	1	1

$$\langle O_1\rangle = \det \mathbf{B} \sum_{k=1}^{4} \sum_{ij} \left(\mathbf{B}^k\right)^{-1}_{ji} \langle \varphi_i(\mathbf{S}_i)|o_1|\varphi_j(\mathbf{S}'_j)\rangle, \tag{1.5.15}$$

where the spin and isospin components of the individual orbitals have been taken out. The number of terms in the summations over ij of course depends on the spin/isposin index k.

Two-body operators in general depend on spin and isospin, but Eq. (1.5.9) can also be simplified. Let us consider a central nucleon–nucleon interaction defined by Eq. (1.2.4). The matrix elements (1.5.9) and (1.5.12) can be written as

$$\begin{aligned}\langle V^{N,c}\rangle = \frac{1}{2} \det \mathbf{B} \sum_{k_1,k_2=1}^{4} \sum_{ijkl} \left(\mathbf{B}^{k_1}\right)^{-1}_{ki} \left(\mathbf{B}^{k_2}\right)^{-1}_{lj} \\ \times \Big[A_D^{k_1k_2} \langle \varphi_i(\mathbf{S}_i)\varphi_j(\mathbf{S}_j)|v|\varphi_k(\mathbf{S}'_k)\varphi_l(\mathbf{S}'_l)\rangle \\ - A_E^{k_1k_2} \langle \varphi_i(\mathbf{S}_i)\varphi_j(\mathbf{S}_j)|v|\varphi_l(\mathbf{S}'_l)\varphi_k(\mathbf{S}'_k)\rangle \Big],\end{aligned} \tag{1.5.16}$$

where v is a Gaussian form factor, and where the direct and exchange coefficients $A_D^{k_1k_2}$ and $A_E^{k_1k_2}$ are defined for each operator in (1.2.4). They are given in Table 1.2, as well as the corresponding coefficients $C_D^{k_1,k_2}$ and $C_E^{k_1,k_2}$ arising from the Coulomb interaction (1.2.2). Notice that these coefficients satisfy the symmetry properties

$$A_D^{k_2k_1} = A_D^{k_1k_2}, \quad A_E^{k_2k_1} = A_E^{k_1k_2}, \tag{1.5.17}$$

and equivalent relations hold for the Coulomb potential. Summations (1.5.16) can therefore be simplified.

1.5.3 The Spin–Orbit Interaction

Potentials considered in the previous section are scalar operators with respect to the spin. For two nucleons coupled to spin $S=0$ or 1 and projection M_S, the application of the Wigner–Eckart theorem gives

$$\langle SM_S|V^{N,c}|S'M'_S\rangle = \langle S||V^{N,c}||S'\rangle\delta_{SS'}\delta_{M_SM'_S}, \tag{1.5.18}$$

where the reduced matrix element $\langle S||V^{N,c}||S'\rangle$ does not depend on the spin projections. The spin–orbit potential is a rank-1 operator, and the previous property does not hold anymore. The calculation of the matrix elements is therefore more complicated since the overlap between wave functions with different spins is zero.

Let us consider the scalar product involved in the spin–orbit potential (1.2.5)

$$\mathbf{L}\cdot\mathbf{S} = L_zS_z + (S_+L_- + S_-L_+)/2. \tag{1.5.19}$$

Since S_z does not change the spin of the a nucleon pair, the contribution of L_zS_z can be determined as in (1.5.16)

$$\begin{aligned}\langle L_zS_z\exp(-(\frac{r}{r_0})^2)\rangle = \frac{1}{2}\det\mathbf{B}\sum_{k_1,k_2}\sum_{ijkl}\left(\mathbf{B}^{k_1}\right)^{-1}_{ki}\left(\mathbf{B}^{k_2}\right)^{-1}_{lj}\\ \times\left[S_D^{k_1k_2}\langle\varphi_i(\mathbf{R}_i)\varphi_j(\mathbf{R}_j)|L_z\exp(-(\frac{r}{r_0})^2)|\varphi_k(\mathbf{R}_k)\varphi_l(\mathbf{R}_l)\rangle\right.\\ \left.-S_E^{k_1k_2}\langle\varphi_i(\mathbf{R}_i)\varphi_j(\mathbf{R}_j)|L_z\exp(-(\frac{r}{r_0})^2)|\varphi_l(\mathbf{R}_l)\varphi_k(\mathbf{R}_k)\rangle\right],\end{aligned} \tag{1.5.20}$$

where coefficients $S_D^{k_1k_2}$ and $S_E^{k_1k_2}$ are given in Table 1.1. The matrix elements of S_+L_- and S_-L_+ must be computed with the more general formula (1.5.9).

1.5.4 Matrix Elements Between Individual Orbitals

We give here matrix elements for $0s$ orbitals [32], and then discuss how to derive matrix elements involving higher shells. As mentioned previously we assume that all orbitals have the same oscillator parameter b. Notation φ_i corresponds to a $0s$ orbital centred at $\mathbf{R}_i$.

The overlap, kinetic energy and r.m.s radius are given by

$$\begin{aligned}\langle\varphi_i|\varphi_j\rangle &= B_{ij} = \exp\left(-\frac{(\mathbf{R}_i-\mathbf{R}_j)^2}{4b^2}\right),\\ \langle\varphi_i|-\frac{\hbar^2}{2m_N}\Delta|\varphi_j\rangle &= \hbar\omega\left[\frac{3}{4}-\frac{(\mathbf{R}_i-\mathbf{R}_j)^2}{8b^2}\right]B_{ij},\\ \langle\varphi_i|r^2|\varphi_j\rangle &= \left[\frac{3}{2}b^2+\frac{(\mathbf{R}_i+\mathbf{R}_j)^2}{4}\right]B_{ij}.\end{aligned} \tag{1.5.21}$$

For a Gaussian form factor and for the Coulomb interaction we have

$$\langle\varphi_i\varphi_j|\exp(-\frac{(\mathbf{r}_1-\mathbf{r}_2)^2}{a^2})|\varphi_k\varphi_l\rangle = \left(\frac{a^2}{a^2+2b^2}\right)^{3/2}\exp\left(-\frac{2b^2}{a^2+2b^2}\mathbf{P}^2\right)B_{ik}B_{jl}, \tag{1.5.22}$$

and

$$\langle\varphi_i\varphi_j|\frac{1}{|\mathbf{r}_1-\mathbf{r}_2|}|\varphi_k\varphi_l\rangle = \frac{1}{\sqrt{2}b}\frac{\mathrm{erf}(P)}{P}B_{ik}B_{jl}, \tag{1.5.23}$$

where vector $\mathbf{P}$ is defined as

$$\mathbf{P} = \frac{1}{2\sqrt{2}b}(\mathbf{R}_i-\mathbf{R}_j+\mathbf{R}_k-\mathbf{R}_l). \tag{1.5.24}$$

For the spin–orbit potential, we need the matrix elements

$$\langle\varphi_i\varphi_j|\exp(-\frac{(\mathbf{r}_1-\mathbf{r}_2)^2}{r_0^2})\mathbf{L}_\mu|\varphi_k\varphi_l\rangle = -\frac{i}{4b^2}\frac{r_0^2}{r_0^2+2b^2}\left[(\mathbf{R}_i-\mathbf{R}_j)\times(\mathbf{R}_k-\mathbf{R}_l)\right]_\mu \times\langle\varphi_i\varphi_j|\exp(-\frac{(\mathbf{r}_1-\mathbf{r}_2)^2}{r_0^2})|\varphi_k\varphi_l\rangle, \tag{1.5.25}$$

where $\mu=-1,0,1$. The combination of (1.2.5), (1.5.22) and (1.5.25) shows that the factors involving r_0 cancel out in the final matrix element of the spin–orbit interaction.Matrix elements involving p orbitals can be obtained by rewriting (1.4.5) as

$$\varphi_{p\mu}(\mathbf{r},\mathbf{R}) = \sqrt{2}b\frac{d}{dR_\mu}\varphi_s(\mathbf{r},\mathbf{R}). \tag{1.5.26}$$

The corresponding matrix elements are therefore obtained by differentiation of $0s$ matrix elements with respect to the generator coordinate $\mathbf{R}$. Another approach is to expand harmonic-oscillator orbitals in a Cartesian basis. Matrix elements in this basis can be computed by recurrence relations [90]. In practice the latter technique is the most efficient to include orbitals beyond the p shell.

1.5.5 Example: α + n Overlap Kernel

In this section we present an illustrative example with the α + n system, treated in a way which is adopted in numerical calculations. Similar developments are presented in Ref. [31] for the $\alpha+\alpha$ system. More general results, obtained for systems involving an α particle and an s-shell cluster will be given in the next subsection. The α particle is built with four $0s$ orbitals, whereas the external neutron can have a spin up or down. As long as the interaction does not depend on the spin, both projections are

not coupled.As in Sect. 1.3.2, we define a Slater determinant with $m_s = -1/2$ for the external neutron. The GCM basis function (1.4.7) is explicitly written as

$$\Phi(\mathbf{R}) = \frac{1}{\sqrt{5!}} \times \det\{\varphi_{0s}(-\frac{\mathbf{R}}{5})n\downarrow \varphi_{0s}(-\frac{\mathbf{R}}{5})n\uparrow \varphi_{0s}(-\frac{\mathbf{R}}{5})p\downarrow \varphi_{0s}(-\frac{\mathbf{R}}{5})p\uparrow \varphi_{0s}(\frac{4\mathbf{R}}{5})n\downarrow\}, \tag{1.5.27}$$

where we use $\lambda = 1/5$, which makes the c.m. factor (1.4.12) equal to unity. The overlap between two Slater determinants (1.5.27) is therefore given by

$$N(\mathbf{R},\mathbf{R}') = \langle\Phi(\mathbf{R})|\Phi(\mathbf{R}')\rangle = \begin{vmatrix} B_{11} & B_{12} & 0 & 0 & 0 \\ B_{21} & B_{22} & 0 & 0 & 0 \\ 0 & 0 & B_{11} & 0 & 0 \\ 0 & 0 & 0 & B_{11} & 0 \\ 0 & 0 & 0 & 0 & B_{11} \end{vmatrix}$$
$$= B_{11}^3(B_{11}B_{22} - B_{12}B_{21}), \tag{1.5.28}$$

with

$$\begin{aligned} B_{11} &= \langle\varphi_{0s}(-\frac{1}{5}\mathbf{R})|\varphi_{0s}(-\frac{1}{5}\mathbf{R}')\rangle \\ B_{12} &= \langle\varphi_{0s}(-\frac{1}{5}\mathbf{R})|\varphi_{0s}(\frac{4}{5}\mathbf{R}')\rangle \\ B_{21} &= \langle\varphi_{0s}(\frac{4}{5}\mathbf{R})|\varphi_{0s}(-\frac{1}{5}\mathbf{R}')\rangle \\ B_{22} &= \langle\varphi_{0s}(\frac{4}{5}\mathbf{R})|\varphi_{0s}(\frac{4}{5}\mathbf{R}')\rangle. \end{aligned} \tag{1.5.29}$$

Using the single-particle overlap (1.5.21), we find

$$N(\mathbf{R},\mathbf{R}') = \exp\left(-\frac{(\mathbf{R}-\mathbf{R}')^2}{5b^2}\right)\left[1 - \exp\left(-\frac{\mathbf{R}\cdot\mathbf{R}'}{2b^2}\right)\right]. \tag{1.5.30}$$

The first term is the direct contribution, which stems from the diagonal of the overlap matrix. The second term is responsible for exchange effects, and is negligible at large distances. When $\mathbf{R}$ (or $\mathbf{R}'$) tends to zero, the Slater determinant (1.5.27) vanishes since two rows or columns are identical. This property is a consequence of the Pauli principle, and the total overlap (1.5.30) also vanishes.

In this simple example, projection over angular momentum is directly obtained from definition (1.4.31) as

$$N_\ell(R,R') = \frac{1}{4\pi}\exp\left(-\frac{R^2+R'^2}{5b^2}\right)\left[i_\ell\left(\frac{2RR'}{5b^2}\right) - (-1)^\ell i_\ell\left(\frac{RR'}{10b^2}\right)\right]. \tag{1.5.31}$$

1.5.6 GCM Kernels of $\alpha + N$ Systems

In this section we present analytical expressions for $\alpha + N$ GCM kernels, where N is a $0s$ shell nucleus (with A_2 nucleons). An extension to systems involving an ^{16}O core is given in Ref. [81]. As shown by Horiuchi [32] (see also Ref. [88]), the overlap kernel takes the general form

$$N(\mathbf{R}, \mathbf{R}') = \sum_{n=0}^{A_2} N_n f_n(\mathbf{R}, \mathbf{R}'), \tag{1.5.32}$$

with

$$f_n(\mathbf{R}, \mathbf{R}') = \exp\left(-\frac{\mu_0 \nu}{2}(\mathbf{R} - \mathbf{R}')^2 - n\nu \mathbf{R} \cdot \mathbf{R}'\right), \tag{1.5.33}$$

and $\nu = 1/2b^2$. Index n in (1.5.32) can be interpreted as the number of exchanged terms. The overlap kernel is therefore entirely determined from a set of integer numbers N_n. They can be obtained from algebraic calculations.

For the symmetric $\alpha + \alpha$ system ($\mu_0 = 2$), functions f_n must be symmetrized as

$$f_n(\mathbf{R}, \mathbf{R}') \to \frac{1}{2}\left(f_n(\mathbf{R}, \mathbf{R}') + f_n(\mathbf{R}, -\mathbf{R}')\right), \tag{1.5.34}$$

which shows that terms corresponding to n and $4 - n$ are equivalent in expansion (1.5.32). After expansion on angular momentum, the symmetrized definition (1.5.34) involves even partial waves only.

For systems involving $0s$-shell orbitals, the kinetic energy matrix element between individual orbitals φ_i can be written as [see Eq. (1.5.21)]

$$\langle \varphi_i | -\frac{\hbar^2}{2m_N}\Delta | \varphi_j \rangle = \hbar\omega \left[\frac{3}{4}\langle \varphi_i | \varphi_j \rangle + \frac{\nu}{2}\frac{d}{d\nu}\langle \varphi_i | \varphi_j \rangle\right]. \tag{1.5.35}$$

Consequently, the kinetic-energy kernel reads, after subtraction of the c.m. contribution,

$$T(\mathbf{R}, \mathbf{R}') = \hbar\omega \left[\frac{3}{4}(A-1) + \frac{\nu}{2}\frac{d}{d\nu}\right] N(\mathbf{R}, \mathbf{R}'), \tag{1.5.36}$$

and can be directly obtained from coefficients N_n. These coefficients are given in Table 1.3 for various systems.

For the potential kernels, we assume that the nuclear interaction is given by combinations of Gaussian functions and exchange operators O as

$$v^N(r) = V_0 \exp\left(-\frac{r^2}{a^2}\right) O, \tag{1.5.37}$$

Table 1.3 Coefficients N_n of the overlap kernel

System	$n=0$	$n=1$	$n=2$	$n=3$	$n=4$
$\alpha+n$, $\alpha+p$	1	−1			
$\alpha+{}^3$H, $\alpha+{}^3$He	1	−3	3	−1	
$\alpha+\alpha$	1	−4	6	−4	1

where O is one of the operators 1, $P^\sigma P^\tau$, P^σ, P^τ. The GCM kernel corresponding to the two-body potential (1.5.37) is given by (see Ref. [32])

$$V^N(\mathbf{R},\mathbf{R}') = V_0\left(\frac{a^2}{a^2+2b^2}\right)^{3/2}\sum_n f_n(\mathbf{R},\mathbf{R}')\sum_{i=1}^{5} V_{ni}^N \exp[-\alpha^2 F_i^2(\mathbf{R},\mathbf{R}')], \tag{1.5.38}$$

where functions $F_i(\mathbf{R},\mathbf{R}')$ are defined as

$$\begin{aligned} F_1(\mathbf{R},\mathbf{R}') &= 0,\\ F_2(\mathbf{R},\mathbf{R}') &= \mathbf{R}/2\sqrt{2}b,\\ F_3(\mathbf{R},\mathbf{R}') &= \mathbf{R}'/2\sqrt{2}b,\\ F_4(\mathbf{R},\mathbf{R}') &= (\mathbf{R}+\mathbf{R}')/2\sqrt{2}b,\\ F_5(\mathbf{R},\mathbf{R}') &= (\mathbf{R}-\mathbf{R}')/2\sqrt{2}b, \end{aligned} \tag{1.5.39}$$

and α is defined by $\alpha^2 = 2b^2/(a^2+2b^2)$.

The Coulomb kernel takes the general form

$$V^C(\mathbf{R},\mathbf{R}') = \frac{e^2}{\sqrt{2}b}\sum_n f_n(\mathbf{R},\mathbf{R}')\sum_{i=1}^{5} V_{ni}^C \frac{\mathrm{erf}[|F_i(\mathbf{R},\mathbf{R}')|]}{|F_i(\mathbf{R},\mathbf{R}')|}. \tag{1.5.40}$$

Coefficients V_{ni}^N and V_{ni}^C are given in Tables 1.4 and 1.5, respectively. The projected kernels are directly obtained by integration over the relative angle between $\mathbf{R}$ and $\mathbf{R}'$ [see Eq. (1.4.31)].

A very simple application is the α particle with four $0s$ orbitals centred at the origin. In that case all space components in (1.5.16) take the same form. For a Gaussian potential of range a and amplitude V_0, the α nuclear and Coulomb energies are

$$\begin{aligned} V^N(\alpha) &= 6(w+m)\left(\frac{a^2}{a^2+2b^2}\right)^{3/2} V_0\\ V^C(\alpha) &= \sqrt{\frac{2}{\pi}}\frac{e^2}{b}. \end{aligned} \tag{1.5.41}$$

Table 1.4 Coefficients V_{ni}^{N} of the nuclear potential for the different exchange operators. The bracketed values correspond to $i=(1,2,3,4,5)$

System	$O=1$	$O=P^{\sigma}P^{\tau}$	$O=P^{\sigma}$	$O=P^{\tau}$
$\alpha+\mathrm{n}, \alpha+\mathrm{p}$				
$n=0$	(6,0,0,4,0)	$(-6, 0, 0, 1, 0)$	(0,0,0, 2,0)	(0, 0, 0, 2, 0)
$n=1$	$(-3, -3, -3, 0, -1)$	$(3, 3, 3, 0, -4)$	$(0, 0, 0, 0, -2)$	$(0, -1, -1, 0, -1)$
$\alpha+^{3}\mathrm{H}, \alpha+^{3}\mathrm{He}$				
$n=0$	(9,0,0,12,0)	$(-9, 0, 0, 3, 0)$	(0,0,0,6,0)	(0,0,0,6,0)
$n=1$	$(-12, -15, -15, -18, -3)$	$(12, 15, 15, -12, -12)$	$(0, 0, 0, -12, -6)$	$(0, 0, 0, -12, -6)$
$n=2$	(9 ,18, 18 ,6 ,12)	$(-9, -18, -18, 9, 18)$	(0 ,0, 0, 6 ,12)	(0 ,0, 0 ,6,12)
$n=3$	$(-6, -3, -3, 0, -9)$	$(6, 3, 3, 0, -6)$	$(0, 0, 0, 0, -6)$	$(0, 0, 0, 0, -6)$
$\alpha+\alpha$				
$n=0$	(12, 0, 0 ,16 ,0)	$(-12, 0, 0, 4, 0)$	(0 ,0 ,0, 8, 0)	(0, 0 ,0 ,8 ,0)
$n=1$	$(-24, -24, -24, -36, -4)$	$(24, 24, 24, -24, -16)$	$(0, 0, 0, -24, -8)$	$(0, 0, 0, -24, -8)$
$n=2$	(24, 48 ,48, 24 ,24)	$(-24, -48, -48, 36, 36)$	(0 ,0, 0 ,24 ,24)	(0 ,0, 0 ,24 ,24)
$n=3$	$(-24, -24, -24, -4, -36)$	$(24, 24, 24, -16, -24)$	$(0, 0, 0, -8, -24)$	$(0, 0, 0, -8, -24)$
$n=4$	(12 ,0 ,0 ,0 ,16)	$(-12, 0, 0, 0, 4)$	(0, 0 ,0 ,0 ,8)	(0, 0, 0, 0 ,8)

Table 1.5 Coefficients V_{ni}^{C} of the Coulomb potential (see caption of Table 1.4). V_{C1} and V_{C2} correspond to the mirror systems

System	V_{C1}	V_{C2}
$\alpha + \mathrm{n}, \alpha + \mathrm{p}$		
$n=0$	(1, 0, 0, 0, 0)	(1,0,0,2,0)
$n=1$	(−1, 0, 0, 0, 0)	(0, −1, −1, 0, −1)
$\alpha +^3$ H, $\alpha +^3$ He		
$n=0$	(2, 0 ,0 ,4 ,0)	(1, 0, 0, 2,0)
$n=1$	(−2, −4, −4, −6, −2)	(−2, −1, −1, −4, −1)
$n=2$	(2, 4, 4 ,2, 6)	(1, 2 ,2, 2 ,2)
$n=3$	(−2, 0, 0, 0, −4)	(0, −1, −1, 0, −1)
$\alpha + \alpha$		
$n=0$	(2, 0 ,0 ,4 ,0)	
$n=1$	(−4, −4, −4, −10, −2)	
$n=2$	(4, 8, 8, 8, 8)	
$n=3$	(−4, −4, −4, −2, −10)	
$n=4$	(2, 0, 0, 0 ,4)	

1.6 Approximations of the RGM

1.6.1 Eigenvalues of the Overlap Kernel

In this Section, we consider other variants of the RGM equation. All are based on the eigenvalues of the overlap kernel [16, 31, 32, 57, 91]. Let us consider the eigenvalue problem

$$\int \mathcal{N}_\ell(\rho, \rho')\chi_{\ell n}(\rho')d\rho' = \mu_{\ell n}\chi_{\ell n}(\rho), \tag{1.6.1}$$

where $\mathcal{N}_\ell(\rho, \rho')$ is the ℓ-projected overlap kernel. In a more compact notation, Eq. (1.6.1) is rewritten as

$$\mathcal{N}_\ell \chi_{\ell n} = \mu_{\ell n}\chi_{\ell n}. \tag{1.6.2}$$

These orthogonal eigenstates $\chi_{\ell n}$ play an important role in approximations [92] and extensions [93] of the RGM. In particular, eigenstates $\chi_{\ell i}(\rho)$ corresponding to $\mu_{\ell i} = 0$ are called forbidden states. These functions are different from zero and present the property

$$\mathcal{A}\phi_1\phi_2\chi_{\ell i}(\rho) = 0, \tag{1.6.3}$$

i.e. they vanish from the action of the antisymmetrizor. They are typical of calculations with identical oscillator parameters. When the oscillator parameters of both

clusters are different, forbidden states ($\mu_{\ell i} = 0$) are replaced by "almost" forbidden states ($\mu_{\ell i}$ small) which induce spurious states in the Schrödinger equation [16, 31, 37]. On the other hand, eigenstates with $\mu_{\ell i} \approx 1$ are weakly affected by exchange effects of the overlap kernel. The eigenvalue distribution therefore provides some insight on the importance of the antisymmetrization.

For some systems, involving a closed-shell nucleus (α, ^{16}O, ^{40}Ca, ...) and an s-shell cluster, the calculation of the eigenvalues is analytical, and only depends of the quantum number [32]

$$N = 2\ell + n. \tag{1.6.4}$$

For example, the $\alpha + n$, $\alpha + t$ and $\alpha + \alpha$ eigenvalues are

$$\mu_N = \begin{cases} 1 - (-1/4)^N & \text{for } \alpha + n \\ 1 - 3(\frac{5}{12})^N + 3(-\frac{1}{6})^N - (-\frac{3}{4})^N & \text{for } \alpha + t \\ 1 - 2^{2-N} + 3\delta_{N,0} & \text{for } \alpha + \alpha \ (N \text{ even}) \end{cases} . \tag{1.6.5}$$

These eigenvalues do not depend of the oscillator parameter. The eigenfunctions are harmonic oscillator orbitals with oscillator parameter $b/\sqrt{\mu_0}$. From the example (1.6.5) we immediately see that the $\alpha + n$ system presents one forbidden state for $\ell = 0$. The reason is that the s orbital is already occupied in the α particle, and is not accessible to the external neutron. The $\alpha + \alpha$ system presents two forbidden states for $\ell = 0$, one for $\ell = 2$, and zero for $\ell \geq 4$.

In general, the eigenvalue problem (1.6.1) cannot be solved analytically. A numerical approach has been proposed by Varga and Lovas [91] who write (1.6.1) in an equivalent form

$$\mathscr{A}\phi_1\phi_2\chi_{\ell n}(\rho) = \mu_{\ell n}\phi_1\phi_2\chi_{\ell n}(\rho), \tag{1.6.6}$$

which shows that $\mu_{\ell n}$ are the eigenvalues of the antisymetrization operator. Expanding $\chi_{\ell n}(\rho)$ over a finite Gaussian basis as

$$\chi_{\ell n}(\rho) = \sum_i c_n^\ell(R_i)\Gamma_\ell(\rho, R_i) \tag{1.6.7}$$

provides the equivalent eigenvalue problem

$$\sum_i c_n^\ell(R_i)\left(\langle\Phi^\ell(R_j)|\Phi^\ell(R_i)\rangle - \mu_{\ell n}\langle\Gamma_\ell(R_j)|\Gamma_\ell(R_i)\rangle\right) = 0. \tag{1.6.8}$$

The first term is the overlap between two projected Slater determinants (1.4.27), whereas the second term corresponds to the direct contribution, and can be calculated analytically as [94]

$$\langle\Gamma_\ell(R_j)|\Gamma_\ell(R_i)\rangle = \exp\left[-\frac{\mu_0}{4b^2}(R_i^2 + R_j^2)\right] i_\ell\left(\frac{\mu_0 R_i R_j}{2b^2}\right). \tag{1.6.9}$$

Of course, the method is approximative only, but is quite simple to apply, in particular for multicluster problems [95], or in two-cluster systems with different oscillator parameters [37].

1.6.2 Reformulation of the RGM Equation

Our aim here is to reformulate the RGM equation (1.3.17) in a more transparent way. One of the reasons is that the RGM two-cluster kernels can be used in multicluster calculations [93, 96], and therefore provide a microscopic framework to multicluster calculations. After projection on angular momentum ℓ, the RGM equation (1.3.17) can be recast as

$$\big(T_\ell + V_\ell - E\mathscr{N}_{E\ell}\big)g_\ell = Eg_\ell, \tag{1.6.10}$$

where T_ℓ is the kinetic energy in partial wave ℓ, and V_ℓ a potential which includes exchange contributions. Equation (1.6.10) resembles a usual two-body Schrödinger equation, but the equivalent potential depends on energy. This is not a problem in two-body calculations, but raises some ambiguities in multicluster models. In that case, cluster-cluster energies are not precisely defined. An iterative procedure has been proposed by Fujiwara et al. [97] but the method was shown to raise conceptual problems in three-body calculations [48].

An elegant and efficient method has been proposed by Suzuki et al. [96] and is briefly explained here. Let us define a modified radial function

$$\begin{aligned}\hat{g}_\ell = \mathscr{N}_\ell^{1/2} g_\ell &= \sum_n \mu_{\ell n}^{1/2} \langle \chi_{\ell n} | g_\ell \rangle \chi_{\ell n} \\ &= g_\ell - \sum_n (1 - \mu_{\ell n}^{1/2}) \langle \chi_{\ell n} | g_\ell \rangle \chi_{\ell n}.\end{aligned} \tag{1.6.11}$$

Since $\mu_{\ell n}$ tend to unity for large n, $\hat{g}_\ell(\rho)$ and $g_\ell(\rho)$ have the same asymptotic behaviour. In addition, $\hat{g}_\ell(\rho)$ is orthogonal to the forbidden states since

$$\langle \chi_{\ell i} | \hat{g}_\ell \rangle = 0 \tag{1.6.12}$$

for $\mu_{\ell i} = 0$. Replacing g_ℓ by

$$g_\ell = \mathscr{N}_\ell^{-1/2} \hat{g}_\ell \tag{1.6.13}$$

in (1.6.10) provides

$$(T_\ell + V_\ell^{RGM}) \hat{g}_\ell = E \hat{g}_\ell, \tag{1.6.14}$$

where V_ℓ^{RGM} is not local, but does not depend on energy. It is defined as

$$\begin{aligned}V_\ell^{RGM} &= \mathscr{N}_\ell^{-1/2} (T_\ell + V_\ell) \mathscr{N}_\ell^{-1/2} - T_\ell \\ &= V_\ell + W_\ell.\end{aligned} \tag{1.6.15}$$

Of course, implicit summations in (1.6.13) and (1.6.15) only include allowed states ($\mu_{\ell n} \neq 0$). The renormalized RGM therefore contains the bare RGM potential V_ℓ,

and an additional contribution W_ℓ. As shown in [96], this term can be computed by an expansion over harmonic-oscillator functions [32].

In Refs. [93, 96], a detailed comparison is performed between the use of renormalized RGM potentials in three-body calculations and fully microscopic calculations with the same nucleon–nucleon interaction. This is done for three typical three-body systems: $^6\mathrm{He} = \alpha + n + n$, $^9\mathrm{Be} = \alpha + \alpha + n$, and $^{12}\mathrm{C} = \alpha + \alpha + \alpha$. The $\alpha + n$ and $\alpha + \alpha$ RGM potentials W_ℓ have been obtained numerically [96]. The binding energies of the ground states are in reasonable agreement with the microscopic energies, but are slightly underestimated. This leads to the suggestion that three-body effects, missing in the renormalized RGM, should be attractive.

This technique opens various possibilities in the microscopic treatment of the nucleus–nucleus interaction. For example, three-body continuum states [98] could be treated with these potentials. In parallel, Continuum Discretized Coupled Channel (CDCC) calculations require a precise description of two and three-body projectiles [99] and could be performed with non-local RGM potentials. On the other hand, the renormalized RGM has been successfully used to compute the triton and hypertriton binding energies from nucleon–nucleon interactions based an a quark cluster model [100].

1.6.3 The Orthogonality Condition Model

The Orthogonality Condition Model (OCM) has been proposed by Saito [92]. The main idea was to simplify the RGM approach, while keeping its microscopic grounds. Let us introduce the projector

$$\Lambda_\ell = 1 - \sum_{i \in PFS} |\chi_{\ell i}\rangle\langle\chi_{\ell i}|, \tag{1.6.16}$$

where the sum runs over the Pauli forbidden states (PFS, $\mu_{\ell i} = 0$). This provides an equivalent RGM equation [16, 92]

$$\Lambda_\ell (T_\ell + V_\ell^{OCM} - E)\hat{g}_\ell = 0, \tag{1.6.17}$$

where the OCM potential is implicitly defined by

$$\mathscr{H}_\ell = \mathscr{N}_\ell^{1/2}(T_\ell + V_\ell^{OCM})\mathscr{N}_\ell^{1/2}. \tag{1.6.18}$$

Equation (1.6.18) is strictly equivalent to (1.3.17). However, the potential V_ℓ^{OCM} has a non-local form. The purpose of the OCM is to include antisymmetrization effects through the operator Λ_ℓ, but to use approximations for the potential [57, 92]. Various methods have been proposed to solve the non-local equation (1.6.17) (see Refs. [92, 94] and references therein).

The OCM equation can still be simplified by replacing (1.6.17) by the local equation

$$(T_\ell + \tilde{V}_\ell - E)\tilde{g}_\ell = 0 \tag{1.6.19}$$

where $\tilde{V}_\ell$ is a local potential [18, 19]. The role of the forbidden states is simulated by additional non-physical states $\tilde{g}_i$ in the potential. Their number depends on the system and on angular momentum [see Eq. (1.6.5) for some systems]. In this way, the orthogonality condition (1.6.12) is replaced by

$$\langle \tilde{g}_i | \tilde{g}_\ell \rangle = 0. \tag{1.6.20}$$

Deep nucleus–nucleus potentials are available in the literature, in particular for $\alpha + \mathrm{n}$ [101] and $\alpha + \alpha$ [102]. The main advantage of the local approximation is its simplicity. The calculation of bound states and phase shifts is straightforward with, for example, the Numerov method [73, 103]. All matrix elements are obtained from one-dimensional integrals. In nuclear astrophysics, many capture reactions have been investigated in this framework (see for example [94, 104]).

1.7 Recent Developments of the GCM

1.7.1 Introduction

For the sake of clarity, the formalism presented in previous sections was simplified as much as possible. In particular, we neglected the spins of the clusters, assumed single-channel problems, and limited the discussion to two-cluster systems. However, the GCM has been significantly extended in two directions, with the goal of improving the description of the system: the extension to multichannel approaches, and to multicluster calculations. We briefly review these two developments. In addition, attention has been paid on the improvement of the cluster wave functions: large shell-model bases [36], and mixing of several shell-model wave functions corresponding to different oscillator parameters [37].

1.7.2 Internal Wave Functions

Microscopic cluster calculations are performed with a shell-model description for the cluster wave functions. The standard shell-model formalism can therefore be used. However, in contrast with shell-model calculations, the definition of the internal wave functions is just a first step of cluster theories. As long as *s* clusters only are involved, the construction of the shell-model states is trivial. In particular, the corresponding wave functions involve a single Slater determinant (except for the deuteron, but this nucleus is poorly described by the shell model).

Going beyond *s*-shell clusters strongly increases the complexity of the calculations. Analytical developments are, in most cases, very difficult and need to be

replaced by entirely numerical approaches. In Ref. [36], we proposed a generalized cluster model, where the cluster wave functions are defined by all p-shell configurations consistent by the Pauli principle. Formally, this can be directly extended to the sd shell or higher (see for example Refs. [105, 106] for applications involving ^{30}Ne and ^{39}Ca clusters), but raises computational problems owing to the large number of Slater determinants and of orbitals involved in the matrix elements.

In practice, cluster calculations are optimized when working in the LS coupling scheme. As shown before, this allows to factorize a Slater determinant in four nucleon types, according to the spin and isospin. In that case, each nucleon orbital (1.4.2) is defined either in a Cartesian basis as

$$\hat{\varphi}_{n_x n_y n_z, m_s m_t}(\mathbf{r}) = \varphi_{n_x}(x)\varphi_{n_y}(y)\varphi_{n_z}(z)|m_s\rangle|m_t\rangle, \tag{1.7.21}$$

or in a spherical basis as

$$\hat{\varphi}_{nlm_\ell, m_s m_t}(\mathbf{r}) = \varphi_{n\ell}(r)Y_\ell^{m_\ell}(\Omega_r)|m_s\rangle|m_t\rangle, \tag{1.7.22}$$

where the space, spin and isospin components have been factorized. In (1.7.22), $\varphi_{n\ell}(r)$ is an harmonic-oscillator radial function [78]. Both bases are equivalent and related to each other by a unitary transform.

An alternative is to use the jj coupling scheme, where the individual orbitals are defined as

$$\hat{\varphi}_{n\ell jm, m_t}(\mathbf{r}) = \varphi_{nl}(r)\big[Y_\ell(\Omega_r) \otimes \chi_s\big]^{jm}|m_t\rangle. \tag{1.7.23}$$

In this option, the overlap (1.5.3) is expressed as the product of two determinants involving more orbitals (see Sect. 1.5). This property strongly increases the computation times for two-body matrix elements since they involve quadruple sums over the individual orbitals [see (1.5.12)].

Let us now define a Slater determinant built from A_1 individual orbitals. All configurations, compatible with the Pauli principle, must be included up to some excitation level N_{max}. In most cluster calculations, $N_{max} = 0$, but particle-hole excitations $N_{max} > 0$ are possible. A compromise should be adopted between the quality of the internal wave functions and the feasibility of the cluster calculation.

Let us start with the most common applications, i.e. p-shell nuclei with Z_1 protons and N_1 neutrons ($A_1 = Z_1 + N_1$). Filling the p shell can be performed in $N_c = C_6^{Z_1-2} \times C_6^{N_1-2}$ different possibilities (C_i^j is the number of combinations of j elements among i elements). The basis therefore involves N_c Slater determinants Φ_i. For example $N_c = 6$ for ^{15}N, and $N_c = 225$ for ^{12}C.

In general, these shell-model states do not have a definite spin. Projection over the total spin I_1 is performed by diagonalization of the spin operators $\mathbf{I}^2$ and I_z which provides

$$\Phi^{I_1 K_1} = \sum_{i=1}^{N_c} d_i^{I_1 K_1} \Phi_i, \tag{1.7.24}$$

where $d_i^{I_1 K_1}$ are linear coefficients obtained from the eigenvalue problems

$$\sum_{j=1}^{N_c} d_j^{I_1 K_1} \left[\langle \Phi_i \mid \mathbf{I}^2 \mid \Phi_j \rangle - I_1(I_1+1)\delta_{ij} \right] = 0$$
$$\sum_{j=1}^{N_c} d_j^{I_1 K_1} \left[\langle \Phi_i \mid I_z \mid \Phi_j \rangle - K_1 \delta_{ij} \right] = 0. \tag{1.7.25}$$

The fact that the eigenvalues of $\mathbf{I}^2$ and I_z provides integer or half-integer values for I_1 and K_1 is a strong test of the calculation.

In practice, further diagonalizations of the isospin $\mathbf{T}^2$, intrinsic spin $\mathbf{S}^2$ and orbital angular momentum $\mathbf{L}^2$ are performed, in order to obtain a deeper analysis of the wave functions. Basis states (1.7.24) are therefore recombined as

$$\Phi^{I_1 K_1}_{S_1 L_1 T_1 c_1} = \sum_{i=1}^{N_c} d^{I_1 K_1}_{S_1 L_1 T_1 c_1, i} \Phi_i, \tag{1.7.26}$$

where c_1 is an additional quantum number used to distinguish between states with identical values of $(I_1 K_1 S_1 L_1 T_1)$. The parity is simply obtained from the product of the parities of the individual orbitals. Finally, basis states (1.7.26) are used to diagonalize the Hamiltonian. This is necessary in collision theories, where the internal wave functions must be eigenstates of the internal Hamiltonian. Linear combinations of Slater determinants are then used in multicluster calculations.

In principle, wave functions (1.7.26) could be employed for several clusters. In practice, however, the total number of Slater determinants is given by the product of N_c values of each cluster. Consequently calculations are currently limited to systems involving a single cluster with generalized shell-model wave functions (1.7.26). In Ref. [36], we give the different sets of quantum numbers for ^{8}Li ($N_c = 120$) and ^{11}B ($N_c = 300$) described in the p shell. These wave functions are used in that reference for a microscopic calculation of the ^{8}Li$(\alpha, \mathrm{n})^{11}$B cross section. In principle, including excited configurations ($N_{max} > 0$) can be performed, but strongly increases the number of Slater determinants.

Let us briefly compare the use of the *LS* coupling (1.7.21) and of the *jj* coupling (1.7.23). There is an orthogonal transform between them and are equivalent as long as all orbitals of a given shell are considered. As discussed above the use of the *jj* coupling increases the computer times. However it allows to keep limited numbers of Slater determinants, even beyond the p shell.

A simple example is provided by ^{14}C, where both coupling modes are illustrated in Fig. 1.2. In the *LS* coupling mode, six neutrons fill the p shell, and four p protons can be combined in $C_6^4 = 15$ combinations. This provides two 0^+ states, one 1^+ state and two 2^+ states. Alternatively, considering the *jj* coupling mode only provides one 0^+ state since the $1p_{3/2}$ subshell is filled. The corresponding spectra obtained with an oscillator parameter $b = 1.6$ fm, and the V2 interaction ($M = 0.6$) complemented by a spin–orbit force ($S_0 = 30$ MeV.fm^5) are displayed in Fig. 1.3, and compared

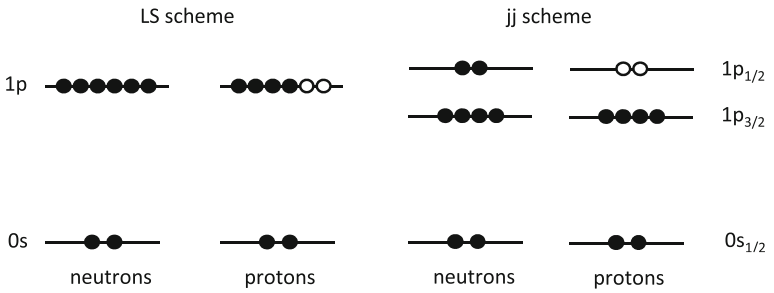

Fig. 1.2 Shell-model orbitals for ^{14}C in the *LS* and *jj* coupling modes (see text). Full and open circles represent occupied and unoccupied orbitals, respectively

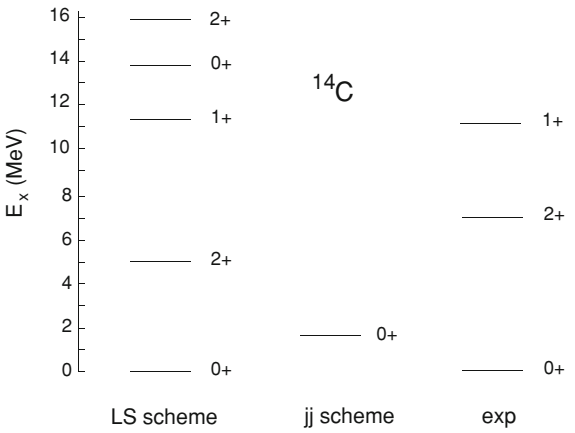

Fig. 1.3 Energy spectrum of ^{14}C in the *LS* and *jj* coupling modes. For the sake of clarity, the experimental energy of the ground state has been shifted to the *LS* value

with experiment. Our goal here is not to optimize the interaction, but to illustrate the problem with a typical nucleon–nucleon force. As expected the *jj* coupling mode, limited to the $1p_{3/2}$ subshell, does not provide excited states and the ground state is less bound (by 1.9 MeV) than in the *LS* coupling mode. The advantage of the former conditions is that the number of Slater determinants is limited to one.

This problem is still more apparent when going to *sd*-shell nuclei. Let us consider ^{17}N, which is illustrated in Fig. 1.4. In the *LS* coupling mode we have $N_c = 6 \times 66 = 396$ Slater determinants. This gives $1/2^-(12)$, $3/2^-(19)$, $5/2^-(18)$ states, $7/2^-(13)$, $9/2^-(6)$, and $11/2^-(2)$ states. The energy spectrum (limited to the 2 first levels for each angular momentum) is shown in Fig. 1.5. Using this set of basis functions for two or three-cluster calculations is highly time and memory consuming. Considering the *jj* coupling mode (illustrated in Fig. 1.4) provides a much smaller number of Slater determinants $N_c = 30$. Of course the number of ^{17}N states is reduced, and the binding energies are lower that in the *LS* coupling mode, but

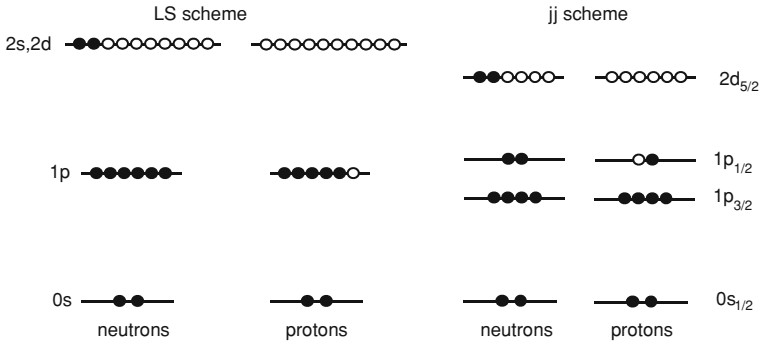

Fig. 1.4 See caption to Fig. 1.2 for ^{17}N

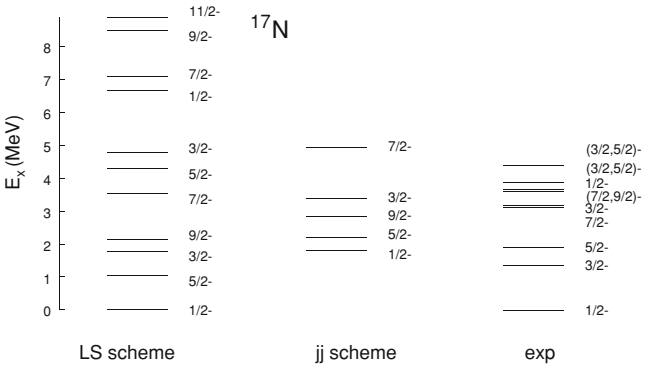

Fig. 1.5 See caption to Fig. 1.3 for ^{17}N

a multicluster calculation (e.g. $^{17}\mathrm{N} + \mathrm{n}$) keeps the computer requirements within acceptable limits. Notice that the calculations have been performed with standard parameters in the nucleon–nucleon interaction. The comparison with experiment can be improved by slightly tuning the parameters M and S_0.

As a general statement, this problem gets more and more important when the nucleon number is far from a closed shell. For example, ^{18}O and ^{30}Ne need $N_c = C_{12}^2 = 66$ in the *sd* shell; in contrast ^{24}Mg would need $N_c = C_{12}^4 \times C_{12}^4 = 245025$, as 4 neutrons and 4 protons are distributed among the 12 *sd* orbitals. If this large number does not raise significant problems in shell-model calculations, it makes cluster approaches impossible owing to the additional clusters, and to the global angular-momentum projection. The use of the *jj* coupling mode, in that case, is necessary.

1.7.3 Multicluster Angular-Momentum Projection

Cluster wave functions based on Slater determinants are not defined with a definite spin value. In order to restore the spin, an angular-momentum projection is needed. We start by assuming that the individual clusters have a spin zero. A projected wave function of the system is obtained from (see Ref. [4])

$$\Phi_K^{LM}(\mathbf{S}_{\{N\}}) = \int \mathscr{D}_{MK}^{L*}(\Omega)\mathscr{R}^L(\Omega)\Phi(\mathbf{S}_{\{N\}})d\Omega, \tag{1.7.27}$$

where $\mathscr{D}_{MK}^L(\Omega)$ is a Wigner function depending on the Euler angles $\Omega = (\alpha, \beta, \gamma)$, and $\Phi(\mathbf{S}_{\{N\}})$ is a N-cluster Slater determinant (1.5.2). In (1.7.27), K is the projection over the intrinsic axis, and the rotation operator $\mathscr{R}^L(\Omega)$ is defined as

$$\mathscr{R}^L(\Omega) = e^{i\alpha L_z}e^{i\beta L_y}e^{i\gamma L_z}, \tag{1.7.28}$$

and performs a rotation of the wave function, or an inverse rotation [107] of the space coordinates $\mathbf{r}_i$ of the individual orbitals. Since the orbitals are defined in the harmonic-oscillator model, a rotation of the quantal coordinates $\mathbf{r}_i$ is equivalent to an inverse rotation of the generator coordinate. Consequently, we have

$$\begin{aligned}\mathscr{R}^L(\Omega)\Phi(\mathbf{S}_{\{N\}}, \mathbf{r}_1, \ldots, \mathbf{r}_A) &= \Phi(\mathbf{S}_{\{N\}}, \mathscr{R}^L(\Omega^{-1})\mathbf{r}_1, \ldots, \mathscr{R}^L(\Omega^{-1})\mathbf{r}_A) \\ &= \Phi(\mathscr{R}^L(\Omega)\mathbf{S}_{\{N\}}, \mathbf{r}_1, \ldots, \mathbf{r}_A).\end{aligned} \tag{1.7.29}$$

The effect of the rotation operator is therefore equivalent to a rotation of the generator coordinates. This property is typical of harmonic oscillator functions, and greatly simplifies the calculations.

Let us consider a rotation-invariant operator O, such that

$$O = \mathscr{R}^L(\Omega^{-1})O\mathscr{R}^L(\Omega). \tag{1.7.30}$$

A matrix element of O between projected functions (1.7.27) reads

$$\begin{aligned}&\langle\Phi_K^{LM}(\mathbf{S}_{\{N\}})|O|\Phi_{K'}^{L'M'}(\mathbf{S}'_{\{N\}})\rangle \\ &= \frac{8\pi^2}{2L+1}\delta_{LL'}\delta_{MM'}\int \mathscr{D}_{KK'}^{L\star}(\omega)\langle\Phi(\mathbf{S}_{\{N\}})|O\mathscr{R}^L(\omega)|\Phi(\mathbf{S}'_{\{N\}})\rangle d\omega,\end{aligned} \tag{1.7.31}$$

and therefore reduces to a three-dimensional integral over the Euler angles. If $O_{\lambda\mu}$ is an irreducible operator of rank λ, (1.7.30) is generalized as

$$\mathscr{R}^L(\Omega)O_{\lambda\mu}\mathscr{R}^L(\Omega^{-1}) = \sum_{\mu} \mathscr{D}_{\mu'\mu}^{\lambda}(\Omega)O_{\lambda\mu'}, \tag{1.7.32}$$

and the matrix element (1.7.31) must be extended [35].

Let us now consider clusters with spin. An N-cluster basis function (which can be a linear combination, as in Sect. 1.7.2) therefore involves quantum numbers associated

with the spin projection K_i and is denoted as $\Phi_{K_1 \ldots K_N}$. In that case, the rotation operator corresponding to the total angular momentum J is factorized as

$$\mathscr{R}^J(\Omega) = \mathscr{R}^L(\Omega)\mathscr{R}^S(\Omega), \tag{1.7.33}$$

where $\mathscr{R}^L(\Omega)$ rotates the space coordinates, and $\mathscr{R}^S(\Omega)$ the spin coordinates. Since, by definition, the cluster states have good spin, the spin rotation provides

$$\mathscr{R}^S(\Omega)\Phi_{K_1 \ldots K_N} = \sum_{K'_1 \ldots K'_N} \mathscr{D}^{I_1}_{K'_1 K_1}(\Omega) \ldots \mathscr{D}^{I_N}_{K'_N K_N}(\Omega)\Phi_{K'_1 \ldots K'_N}, \tag{1.7.34}$$

where I_i are the spins of the N clusters (for the sake of clarity the generator coordinates are implied). A projected basis state (1.7.27) is then generalized to

$$\Phi^{JM}_{K,K_1 \ldots K_N} = \sum_{K'_1 \ldots K'_N} \int \mathscr{D}^{J*}_{KM}(\Omega)\mathscr{D}^{I_1}_{K'_1 K_1}(\Omega) \ldots \mathscr{D}^{I_N}_{K'_N K_N}(\Omega)\mathscr{R}^L(\Omega)\Phi_{K'_1 \ldots K'_N} d\Omega, \tag{1.7.35}$$

and, as in (1.7.27), only the space rotation should be explicitly performed. Matrix elements between functions (1.7.35) are directly obtained from an extension of (1.7.31). Specific applications to 3 and 4-cluster systems can be found in Refs. [35, 108]. An important application concerns two-cluster systems, and is explained in more detail in the next subsection.

Finally the parity projection is performed with the operator

$$\Phi^{JM\pi}_{K,K_1 \ldots K_N} = \frac{1}{2}\big(1 + \pi P\big)\Phi^{JM}_{K,K_1 \ldots K_N}, \tag{1.7.36}$$

where $\pi = \pm 1$ is the parity of the state, and where P reverses all nucleon coordinates as $\mathbf{r}_i \rightarrow -\mathbf{r}_i$. In some specific cases, this operator can be replaced by an equivalent rotation operator (see an example in Ref. [35]). This allows to combine angular-momentum and parity projection in a single rotation operator.

1.7.4 Multichannel Two-Cluster Systems

Until now the presentation was limited to single-channel two-cluster models. We briefly show here how to extend the formalism to multichannel calculations, and/or with spins different from zero. Although the notations are more complicated, the principles of the GCM (Sect. 1.4), as well as matrix elements between basis states (Sect. 1.5) remain unchanged.

Let us consider a channel c composed of two clusters with spins I_1 and I_2 (parities π_1 and π_2 are implied). The internal wave functions $\Phi_c^{I_1 K_1}$ and $\Phi_c^{I_2 K_2}$ are defined in (1.4.1), and are in general combinations of Slater determinants [see (1.7.24)]. A channel c is characterized by the properties of the clusters: masses and charges,

spins, levels of excitation, etc. In transfer and inelastic reactions, the introduction of excited channels is of course necessary. However, even in spectroscopic calculations, additional channels may improve the total wave function of the system, according to the variational principle. As shown in Sect. 1.7.2, calculations involving *p*-shell or *sd*-shell clusters may contain a large number of channels.

From the internal cluster wave functions, we extend definition (1.4.7) to

$$\begin{aligned}\Phi_c^{IK}(\mathbf{R}) &= \frac{1}{\sqrt{N_0}} \sum_{K_1 K_2} \langle I_1 K_1 I_2 K_2 | IK \rangle \mathscr{A} \Phi_c^{I_1 K_1}\left(-\frac{A_2}{A}\mathbf{R}\right) \Phi_c^{I_2 K_2}\left(\frac{A_1}{A}\mathbf{R}\right) \\ &= \frac{1}{\sqrt{N_0}} \mathscr{A}\left[\Phi_c^{I_1}\left(-\frac{A_2}{A}\mathbf{R}\right) \otimes \Phi_c^{I_2}\left(\frac{A_1}{A}\mathbf{R}\right)\right]^{IK}, \end{aligned} \tag{1.7.37}$$

where I is the channel spin, and results from the coupling of I_1 and I_2. This quantum number plays an important role in reactions. In (1.7.37), we assume that the origin is at the c.m., and we have rewritten the angular-momentum coupling in the standard, compact, notation.

According to (1.7.34), projection of basis functions (1.7.37) provides

$$\Phi_{cIK}^{JM}(R) = \int \mathscr{D}_{MK}^{J*}(\Omega) \mathscr{R}^J(\Omega) \Phi_c^{IK}(\mathbf{R}) d\Omega. \tag{1.7.38}$$

This definition is well adapted to spectroscopy. However we define an equivalent basis as

$$\Phi_{c\ell I}^{JM\pi}(R) = \left(\frac{2\ell+1}{256\pi^5}\right)^{1/2} \sum_K \langle IK\ell 0 | JK \rangle \Phi_{cIK}^{JM}(R), \tag{1.7.39}$$

which makes use of the relative angular momentum ℓ. The normalization factor allows to simplify the RGM wave function (see below). This factor, however, can be chosen arbitrarily as long as it is consistent in all matrix elements. Notice that the projection over ℓ directly provides the projection on parity which is related to the individual parities of the clusters π_1 and π_2 as

$$\pi = \pi_1 \pi_2 (-1)^\ell. \tag{1.7.40}$$

Using Eqs. (1.7.27), (1.7.33) and (1.7.34), we have

$$\Phi_{c\ell I}^{JM\pi}(R) = \frac{1}{4\pi} \int d\Omega_R \left[\Phi_c^I(R, \Omega_R) \otimes Y_\ell(\Omega_R)\right]^{JM}. \tag{1.7.41}$$

with

$$\Phi_c^{IK}(R, \Omega_R) = \mathscr{R}^L(\Omega_R) \Phi_c^{IK}(\mathbf{R}). \tag{1.7.42}$$

The overlap between two projected basis functions (1.7.41) is obtained from a generalization of the single-channel result (1.7.31) as

$$\langle \Phi^{J\pi}_{c\ell I}(R) \mid \Phi^{J\pi}_{c'\ell' I'}(R')\rangle = \frac{\sqrt{(2\ell+1)(2\ell'+1)}}{8\pi(2J+1)} \times \sum_{K,K'} \langle I\,K\,\ell\,0 \mid J\,K\rangle \langle I'\,K'\,\ell'\,K-K' \mid J\,K\rangle \times \int_0^\pi d^{\ell'}_{K-K',0}(\beta) \langle \Phi^{IK}_c(R,0) \mid \Phi^{I'K'}_{c'}(R',\beta)\rangle d\cos\beta, \tag{1.7.43}$$

where $\Phi^{IK}_c(R,\beta)$ is a Slater determinant with the generator coordinate in the xz plane, and making an angle β with the z axis. To derive (1.7.43), we have used the symmetry of the unprojected matrix element around the z axis. For two-cluster calculations these matrix elements are obtained from one-dimensional integrals. This definition is valid for any rotation–invariant operator. The extension to more general operators can be found in Ref. [85]. Notice that the projected matrix elements (1.7.43) must be symmetric. This is not trivial since the generator coordinates R and R' are not treated in the same way (R is chosen along the z axis). The symmetry of the final result is a severe test of the calculation.

A calculation analog to those developed in Sect. 1.4 provides the equivalence between the GCM and RGM for a multichannel system. The extension of (1.4.27) is directly obtained from

$$\Phi^{JM\pi}_{c\ell I}(R) = \frac{1}{\sqrt{N_0}} \Phi_{cm} \mathscr{A}\, \Gamma_\ell(\rho,R) \varphi^{JM\pi}_{c\ell I}(\boldsymbol{\xi}_1,\boldsymbol{\xi}_2,\Omega_\rho), \tag{1.7.44}$$

where the channel wave function reads

$$\varphi^{JM\pi}_{c\ell I}(\boldsymbol{\xi}_1,\boldsymbol{\xi}_2,\Omega_\rho) = \left[\left[\phi^{I_1}_c(\boldsymbol{\xi}_1)\otimes\phi^{I_2}_c(\boldsymbol{\xi}_2)\right]^I \otimes Y_\ell(\Omega_\rho)\right]^{JM}. \tag{1.7.45}$$

In this definition, $\phi^{I_1}_c$ and $\phi^{I_2}_c$ are the translation-invariant internal wave functions depending on the sets $\boldsymbol{\xi}_1$ and $\boldsymbol{\xi}_2$ of internal coordinates. In multichannel problems, the total wave function of the system is given by

$$\Psi^{JM\pi} = \sum_{c\ell I} \Psi^{JM\pi}_{c\ell I}, \tag{1.7.46}$$

where the contribution of each channel is defined as

$$\begin{aligned} \Psi^{JM\pi}_{c\ell I} &= \int f^{J\pi}_{c\ell I}(R) \Phi^{JM\pi}_{c\ell I}(R) dR \qquad \text{(in the GCM)} \\ &= \mathscr{A}\, g^{J\pi}_{c\ell I} \varphi^{JM\pi}_{c\ell I} \qquad \text{(in the RGM)}. \end{aligned} \tag{1.7.47}$$

As for single-channel calculations, the RGM radial function is deduced from the generator function as

$$g^{J\pi}_{c\ell I}(\rho) = \int f^{J\pi}_{c\ell I}(R) \Gamma_\ell(\rho,R) dR. \tag{1.7.48}$$

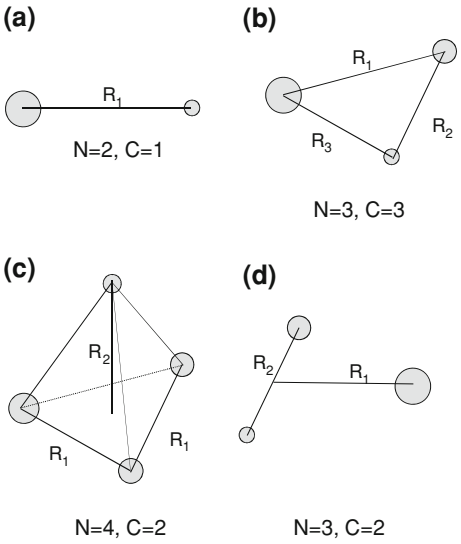

Fig. 1.6 Multicluster configurations for two (**a**), three (**b, d**), and five (**c**) -cluster description. In model (**c**) the basis of the tetrahedron is assumed to be defined by three α particles in an equilateral configuration

1.7.5 Multicluster Models

1.7.5.1 General Discussion

Although multicluster theories have been also developed in the RGM [33], we focus here on GCM calculations. Let us assume N clusters with internal wave functions Φ_N and centered at $\mathbf{S}_i$. As in Sect. 1.5, the set of cluster locations is denoted as $\mathbf{S}_{\{N\}} = (\mathbf{S}_1, \ldots, \mathbf{S}_N)$. From these locations, we define a set of generator coordinates $\mathbf{R}_{\{C\}} = (\mathbf{R}_1, \ldots, \mathbf{R}_C)$ where C represents the number of independent coordinates required to define the system (see Fig. 1.6). For example, two-cluster systems are characterized by one generator coordinate, the distance between the clusters (Fig. 1.6a). In a three-body model, the clusters are located at the vertices of a triangle (Fig. 1.6b). Depending on the geometry of the triangle, the number of generator coordinates can be $C = 1$, 2, or 3 ($C = 1$ for an equilateral triangle).

A GCM basis function is defined by a multicluster generalization of Eq. (1.4.7) as

$$\Phi(\mathbf{R}_{\{C\}}) = \sqrt{\frac{A_1! \cdots A_N!}{A!}} \Phi_{cm}^{-1} \mathscr{A} \Phi_1(\mathbf{S}_1) \ldots \Phi_N(\mathbf{S}_N), \tag{1.7.49}$$

where the c.m. component has been removed. Again, for the sake of clarity, we do not explicitly mention the spin orientations of the clusters. Equation (1.7.49) is the starting point of all multicluster models. Matrix elements between these Slater determinants are obtained as for two-cluster calculations (see Sect. 1.5). When $N > 2$, there are, however, various applications of multicluster models, which differ by the projection technique:

(i) *Systems with a fixed geometry* (Fig. 1.6b for $N=3$ and Fig. 1.6c for $N=4$). Wave function (1.7.49) is projected with (1.7.35) and (1.7.36) on spin J and parity π, respectively. Examples for three-cluster systems are ^{11}Li or ^{24}Mg described by triangular ^{9}Li+n+n or ^{16}O+α+α configurations [109, 110]. Some four-cluster systems have been described by a tetrahedral configuration with an equilateral triangle for the three α particles, and an additional s cluster [35]. The use of a symmetric structure for the three α particles allows a reduction of the computer times for the projected matrix elements.

(ii) *Two-body systems involving a cluster nucleus* (Fig. 1.6d). This approach is essentially used to describe nucleus–nucleus collisions, where one of the colliding nuclei presents a cluster structure. Typical examples are ^{7}Be + p, with ^{7}Be = α + ^{3}He [111] and ^{12}C + α with ^{12}C = 3α [108]. In that case, the angular momentum of the cluster subsystem must be restored. The projection over angular momentum is therefore multiple.

(iii) *Multicluster hyperspherical formalism*. This development is recent [45] and is currently limited to three-cluster systems. The relative motion is described in hyperspherical coordinates [23]. This framework was recently extended to a microscopic description of three-body scattering states [95].

1.7.5.2 Fixed Geometry

In option (i), the projections over angular momentum and parity are performed with (1.7.35) and (1.7.36), respectively. As mentioned before, in some specific cases, the parity P operator can be replaced by a rotation (for example, operator P in an equilateral triangle involving three identical clusters is equivalent to a rotation by π). When the clusters have a spin zero, a projected matrix element of a rotation-invariant operator O between projected basis functions (1.7.27) is obtained from (1.7.31). The integrals are in general performed numerically (see Ref. [35] for further detail).

Finally, the total wave function of the system is obtained from a superposition of projected functions (1.7.27) as

$$\begin{aligned}\Psi^{JM\pi} &= \sum_K \int f_K^{J\pi}(R_{\{C\}})\Phi_K^{JM\pi}(R_{\{C\}})dR_1\cdots dR_C,\\ &\approx \sum_K \sum_{R_{\{C\}}} f_K^{J\pi}(R_{\{C\}})\Phi_K^{JM\pi}(R_{\{C\}}).\end{aligned} \tag{1.7.50}$$

Coefficients $f_K^{J\pi}(R_{\{C\}})$ are obtained from the Hill–Wheeler involving the Hamiltonian and overlap kernels

$$\sum_{R'_{\{C\}},K'} \left[H_{KK'}^{J\pi}(R_{\{C\}},R'_{\{C\}}) - E_\omega^{J\pi} N_{KK'}^{J\pi}(R_{\{C\}},R'_{\{C\}})\right] f_{K'}^{J\pi}(R'_{\{C\}}) = 0. \tag{1.7.51}$$

When the cluster spins are different from zero, additional quantum numbers, corresponding to the spin orientations, must be introduced. This model is well adapted

to three-body halo nuclei, such as ^{6}He [112] or ^{11}Li [109]. The 3α and 4α descriptions of ^{12}C and ^{16}O are also known to significantly improve the binding energies [35].

1.7.5.3 Systems Involving a Cluster Nucleus

Multicluster models mentioned in the previous subsection are well adapted to nuclear spectroscopy. To extend these models to nucleus–nucleus reactions, a multiple angular momentum is necessary to restore, not only the spin of the total system, but also the spins of the colliding nuclei. Although a situation where both colliding nuclei present a cluster structure is possible, practical applications are currently limited to a *s*-shell particle with a multicluster nucleus. We therefore consider systems built from $N+1$ clusters.

Let us define nucleus 1 by N clusters with a set of generator coordinates $R_{\{C\}}$. The internal wave functions with spins I_1 and parity π_1 are therefore taken as in Eq. (1.7.50) and read

$$\Phi_{\omega}^{I_1 K_1 \pi_1} = \sum_{K, R_{\{C\}}} F_{K,\omega}^{I_1 \pi_1}(R_{\{C\}}) \Phi_{K}^{I_1 K_1 \pi_1}(R_{\{C\}}). \tag{1.7.52}$$

In this definition, index ω corresponds to the level of excitation. Wave functions with different ω values are orthogonal to each other. States with $E_{\omega}^{I_1\pi_1} < 0$ correspond to bound states, whereas $E_{\omega}^{I_1\pi_1} > 0$ represent pseudostates. They can be interpreted as square-integrable approximations of scattering states, and simulate the distortion of the nucleus.

Let us now consider the total $(N+1)$-cluster system. The relative motion with nucleus 2 (assumed to be described by a single cluster) requires the additional relative coordinate R. An unprojected wave function is written as

$$\Phi(\mathbf{R}_{\{C\}}, \mathbf{R}) = \frac{1}{\sqrt{N_0}} \mathscr{A} \Phi_1 \left(\mathbf{R}_{\{C\}}, -\frac{A_2}{A}\mathbf{R} \right) \Phi_2 \left(\frac{A_1}{A}\mathbf{R} \right), \tag{1.7.53}$$

where $\Phi_1(\mathbf{R}_{\{C\}}, -\frac{A_2}{A}\mathbf{R})$ is a Slater determinant (1.7.49) centred at $-\frac{A_2}{A}\mathbf{R}$. After projection over the angular momentum of nucleus 1, and summation over $R_{\{C\}}$, a basis state is defined as

$$\Phi_{\omega}^{IK}(\mathbf{R}) = \frac{1}{\sqrt{N_0}} \mathscr{A} [\Phi_{\omega}^{I_1\pi_1}(-\frac{A_2}{A}\mathbf{R}) \otimes \Phi^{I_2\pi_2}(\frac{A_1}{A}\mathbf{R})]^{IK}, \tag{1.7.54}$$

where (1.7.52) has been used for nucleus 1. The multichannel theory presented in Sect. 1.7.4 can therefore be applied. In particular the matrix elements (1.7.43) are still valid, after an additional projection on $I_1\pi_1$. In general, these matrix elements involve 7-dimensional integrals [80, 113] (3 dimensions for the Euler angles in the bra and in the ket, and one additional integral for the relative motion). When the cluster nucleus involves two clusters, this integral is reduced to 5 dimensions [110].

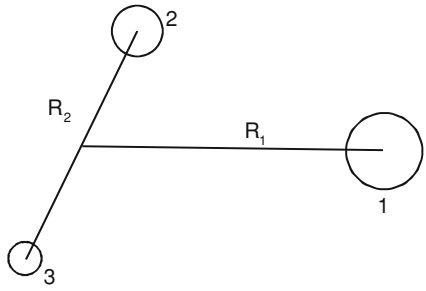

Fig. 1.7 Three-cluster configuration

1.7.5.4 Hyperspherical Formalism

Let us consider the three-cluster system displayed in Fig. 1.7. The center of mass of each cluster is defined as

$$\begin{aligned}\mathbf{R}_{cm,1} &= \frac{1}{A_1}\sum_{i=1}^{A_1}\mathbf{r}_i,\\ \mathbf{R}_{cm,2} &= \frac{1}{A_2}\sum_{i=A_1+1}^{A_1+A_2}\mathbf{r}_i,\\ \mathbf{R}_{cm,3} &= \frac{1}{A_3}\sum_{i=A_1+A_2+1}^{A}\mathbf{r}_i.\end{aligned} \tag{1.7.55}$$

In the hyperspherical formalism [23], the scaled Jacobi coordinates are given by

$$\begin{aligned}\mathbf{x} &= \sqrt{\mu_{23}}(\mathbf{R}_{cm,2}-\mathbf{R}_{cm,3}),\\ \mathbf{y} &= \sqrt{\mu}\left[\mathbf{R}_{cm,1}-\frac{A_2\mathbf{R}_{cm,2}+A_3\mathbf{R}_{cm,3}}{A_{23}}\right],\end{aligned} \tag{1.7.56}$$

where $A_{23}=A_2+A_3$, and where the reduced masses are

$$\begin{aligned}\mu_{23} &= \frac{A_2A_3}{A_{23}}\\ \mu &= \frac{A_1A_{23}}{A}.\end{aligned} \tag{1.7.57}$$

These coordinates provide the hyperradius and hyperangle

$$\begin{aligned}\rho^2 &= \mathbf{x}^2+\mathbf{y}^2\\ \alpha_\rho &= \arctan(y/x).\end{aligned} \tag{1.7.58}$$

The hyperspherical formalism is well known in non-microscopic three-body systems [30, 114], where the structure of the nuclei is neglected. In that case, the kinetic energy can be written as

$$T = -\frac{\hbar^2}{2m_N}\left(\frac{\partial^2}{\partial\rho^2} + \frac{5}{\rho}\frac{\partial}{\partial\rho} - \frac{\mathbf{K}^2(\Omega^5)}{\rho^2}\right), \tag{1.7.59}$$

where $\Omega^5 = (\Omega_x, \Omega_y, \alpha)$ is defined from the hyperangle α, and by the directions of the Jacobi coordinates Ω_x and Ω_y. The hypermomentum operator $\mathbf{K}^2$ generalizes the concept of angular momentum in two-body systems and can be diagonalized as

$$\mathbf{K}^2 \mathscr{Y}^{\ell_x\ell_y}_{KLM}(\Omega^5) = K(K+4)\mathscr{Y}^{\ell_x\ell_y}_{KLM}(\Omega^5), \tag{1.7.60}$$

where $\mathbf{K}$ is the hypermomentum, and ℓ_x and ℓ_y are the orbital momenta associated with $\mathbf{x}$ and $\mathbf{y}$. The hyperspherical functions are [115]

$$\mathscr{Y}^{\ell_x\ell_y}_{KLM}(\Omega^5) = \phi^{\ell_x\ell_y}_K(\alpha)\left[Y_{\ell_x}(\Omega_x) \otimes Y_{\ell_y}(\Omega_y)\right]^{LM}, \tag{1.7.61}$$

with

$$\phi^{\ell_x\ell_y}_K(\alpha) = \mathscr{N}^{\ell_x\ell_y}_K (\cos\alpha)^{\ell_x}(\sin\alpha)^{\ell_y} P_n^{\ell_y+1/2,\ell_x+1/2}(\cos 2\alpha). \tag{1.7.62}$$

In these definition, $P_n^{\alpha\beta}(x)$ is a Jacobi polynomial, $\mathscr{N}^{l_x l_y}_K$ is a normalization factor, and $n = (K - \ell_x - \ell_y)/2$ is a positive integer. The total wave function is then expanded over the basis (1.7.61), which provides a system of coupled differential equations (see Ref. [114] for detail). There are three different choices for the Jacobi coordinates (1.7.56). However, these choices are equivalent since the corresponding hyperspherical functions (1.7.61) are related to each other by a unitary transform involving Raynal–Revai coefficients [115]. Many applications have been performed in the spectroscopy of light nuclei [114, 116] and, more recently, for three-body continuum states [98, 117].

The extension of the hyperspherical theory to microscopic three-cluster systems is recent [45]. Let us consider a three-cluster Slater determinant (1.7.49) or (1.7.53) defined by two generator coordinates $\mathbf{R}_1$ and $\mathbf{R}_2$ (see Fig. 1.7). According to (1.7.58), we define the hyperradius and hyperangle from the scaled generator coordinates

$$\begin{aligned} \mathbf{X} &= \sqrt{\mu_{23}}\,\mathbf{R}_2 \\ \mathbf{Y} &= \sqrt{\mu}\,\mathbf{R}_1 \end{aligned} \tag{1.7.63}$$

as

$$\begin{aligned} R^2 &= \mathbf{X}^2 + \mathbf{Y}^2 \\ \alpha_R &= \arctan(Y/X). \end{aligned} \tag{1.7.64}$$

This Slater determinant can be factorized as in (1.4.8) for two-cluster systems. We have

$$\Phi(\mathbf{X}, \mathbf{Y}) = \Phi_{cm}\mathscr{A}\phi_1\phi_2\phi_3 \exp\left(-\frac{(\mathbf{x}-\mathbf{X})^2}{2b^2}\right)\exp\left(-\frac{(\mathbf{y}-\mathbf{Y})^2}{2b^2}\right), \tag{1.7.65}$$

where Φ_{cm} is defined as in (1.4.19), and ϕ_1, ϕ_2, ϕ_3 are the translation-invariant internal wave functions of the three clusters. We take here the origin of the coordinates at the center of mass. We assume that the clusters have a spin zero, but the theory can be generalized by additional angular momentum couplings (see Ref. [45] for detail).

To develop (1.7.65), we use the expansion [115]

$$\exp\left(-(\mathbf{x}.\mathbf{X}+\mathbf{y}.\mathbf{Y})\right) = \frac{(2\pi)^3}{(\rho R)^2} \sum_{\ell_x\ell_y LMK} I_{K+2}(R\rho)\mathscr{Y}^{\ell_x\ell_y}_{KLM}(\Omega^5_\rho)\mathscr{Y}^{\ell_x\ell_y *}_{KLM}(\Omega^5_R), \tag{1.7.66}$$

where $I_{K+2}(x)$ is a modified Bessel function. The Slater determinant (1.7.65) can therefore be written as

$$\Phi(\mathbf{X},\mathbf{Y}) = \sum_{\ell_x\ell_y LMK} \Phi^{LM}_{\ell_x\ell_y K}(R)\mathscr{Y}^{\ell_x\ell_y}_{KLM}(\Omega^5_R), \tag{1.7.67}$$

where the projected basis function reads

$$\begin{aligned}\Phi^{LM}_{\ell_x\ell_y K}(R) &= \int d\Omega^5_R \mathscr{Y}^{\ell_x\ell_y \star}_{KLM}(\Omega^5_R)\Phi(\mathbf{X},\mathbf{Y}) \\ &= \Phi_{cm}\mathscr{A}\phi_1\phi_2\phi_3 G_K(\rho,R)\mathscr{Y}^{\ell_x\ell_y}_{KLM}(\Omega^5_\rho),\end{aligned} \tag{1.7.68}$$

with

$$d\Omega^5_R = R^5\cos^2\alpha_R \sin^2\alpha_R d\alpha_R d\Omega_X d\Omega_Y, \tag{1.7.69}$$

and

$$G_K(\rho,R) = \left(\frac{b^2}{\rho R}\right)^2 \left(\frac{4\pi}{b^2}\right)^{3/2} \exp\left(-\frac{\rho^2+R^2}{2b^2}\right) I_{K+2}\left(\frac{\rho R}{b^2}\right). \tag{1.7.70}$$

Definition (1.7.68) is a direct extension of (1.4.27), obtained for two-cluster systems. It only depends on a single generator coordinate, the hyperradius R. As in (1.4.27), ρ is the quantal coordinate, and R a parameter which is not affected by antisymmetrization. The total wave function is given, as in (1.4.28) for two-cluster systems, as

$$\Psi^{LM} = \sum_{\ell_x\ell_y K} \int f^L_{\ell_x\ell_y K}(R)\Phi^{LM}_{\ell_x\ell_y K}(R)dR, \tag{1.7.71}$$

where the generator functions $f^L_{\ell_x\ell_y K}(R)$ are obtained from a three-body Hill–Wheeler equation (1.4.32). The matrix elements involving GCM projected functions are computed as in Sect. 1.7.5.3, with a further integral over the hyperangle. This gives, for the overlap,

$$\langle \Phi^{LM}_{\ell_x\ell_y K}(R)|\Phi^{LM}_{\ell'_x\ell'_y K'}(R')\rangle = \int d\alpha_R d\alpha_{R'} \cos^2\alpha_R \sin^2\alpha_R \cos^2\alpha_{R'} \sin^2\alpha_{R'} \times \phi_K^{\ell_x\ell_y}(\alpha_R)\phi_{K'}^{\ell'_x\ell'_y}(\alpha_{R'})\langle \Phi^{L}_{\ell_x\ell_y}(X,Y)|\Phi^{L}_{\ell'_x\ell'_y}(X',Y')\rangle, \tag{1.7.72}$$

where the matrix elements in the integrand are obtained from five dimensional integrals. Matrix elements in the hyperspherical framework therefore involve 7-dimensional integrals. The advantage with respect to the fixed geometry is that this basis involves one generator coordinate only. It has been essentially applied to systems involving s clusters, such as ^{6}He [45], ^{6}Li [45], ^{9}Be [96] or ^{12}C [96]. In that case, a semi-analytic treatment of the matrix elements (1.7.72) can be used. Very recently an ^{16}O+p+p calculation was performed [118] to investigate the diproton radioactivity of ^{18}Ne. The model has also been extended to a microscopic description of three-body continuum states [95].

1.8 Scattering States With the GCM

1.8.1 Introduction

The treatment of scattering states in microscopic models is a delicate problem. Exact solutions of the Schrödinger equation (1.1.1) for positive energies must take account of the asymptotic boundary conditions. Extensions to scattering and resonant states represent however a wide range of applications: elastic and inelastic scattering, transfer, capture, etc. The two latter processes are important in nuclear astrophysics, where the low-energy cross sections relevant to stellar models are in general too small to be measured in laboratory. The need for a precise treatment of unbound states is also crucial in the study of light exotic nuclei, where the ground state is close to the particle-emission threshold, or is unbound. In that case the determination of resonance properties require an extension to scattering states. At large distances, the microscopic Hamiltonian tends to

$$H \to H_1 + H_2 - \frac{\hbar^2}{2\mu}\Delta_\rho + \frac{Z_1 Z_2 e^2}{\rho}. \tag{1.8.1}$$

Consequently, the relative wave function (1.1.4) of a scattering state at energy E tends to, in partial wave ℓm,

$$\Psi^{\ell m}(\boldsymbol{\rho}) \underset{\rho\to\infty}{\longrightarrow} \phi_1\phi_2 Y_\ell^m(\Omega) g^\ell_{\rm ext}(\rho),$$
$$g^\ell_{\rm ext}(\rho) = I_\ell(k\rho) - U_\ell O_\ell(k\rho), \tag{1.8.2}$$

where k is the wave number, and $I_\ell(x) = O^*_\ell(x)$ are incoming and outgoing Coulomb functions [119]. At large distances, antisymmetrization between the colliding nuclei

is negligible. In Eq. (1.8.2), U_ℓ is the collision matrix, which determines the scattering cross sections. In single-channel calculations, U_ℓ is parametrized as

$$U_\ell = \exp(2i\delta_\ell), \tag{1.8.3}$$

where δ_ℓ is the phase shift. It is real in microscopic theories, since nucleon–nucleon interactions are real. In optical models, it can be complex owing to complex optical potentials. In a multichannel problem [120], U_ℓ is a symmetric and unitary matrix whose size is equal to the number of open channels. Here we restrict the presentations to single-channel calculations. An extension can be found in Refs. [85, 121].

In the RGM approach, solutions of (1.3.17) (or its angular-momentum extension) can be derived at positive energies by using finite-difference methods, or by the Lagrange-mesh approach [122, 123]. The GCM variant, however, cannot be directly adapted to scattering states since any finite combination of (projected) Slater determinants (1.4.27) presents a Gaussian behaviour. This problem is addressed by using the microscopic R-matrix method [119, 124], which is briefly described in Sect. 1.8.3.

1.8.2 Cross Sections

The collision matrices U_ℓ provide the elastic cross section. As in previous sections, we only consider systems with spinless particles (see Ref. [124] for a generalization). At the scattering angle $\Omega = (\theta, \phi)$ the elastic cross section is given by

$$\frac{d\sigma_{\rm el.}}{d\Omega} = |f_C(\Omega) + f_N(\Omega)|^2, \tag{1.8.4}$$

where the Coulomb and nuclear amplitudes read

$$\begin{aligned} f_C(\Omega) &= -\frac{\eta}{2k\sin^2\theta/2} e^{2i(\sigma_0 - \eta \ln\sin\theta/2)}, \\ f_N(\Omega) &= \frac{i}{2k}\sum_\ell (2l+1) e^{2i\sigma_l}(1-U_\ell) P_\ell(\cos\theta). \end{aligned} \tag{1.8.5}$$

In these definitions, $\sigma_\ell = \arg\Gamma(\ell+1+i\eta)$ is the Coulomb phase shift, and $\eta = Z_1 Z_2 e^2/\hbar v$ is the Sommerfeld parameter (v is the relative velocity). As the Coulomb amplitude diverges at small angles, the integrated elastic cross section is not defined for charged-particle scattering.

Radiative capture is an electromagnetic transition from a scattering state to a bound state. The electromagnetic aspects of this process can be studied at the first order of the perturbation theory [119], with a scattering state at positive energy E and a bound state in partial wave $J_f\pi_f$ as final state at negative energy E_f. The definition of capture cross sections can be found in Refs. [124, 125] for example.

1.8.3 The Microscopic R-Matrix Method

As mentioned before, GCM basis functions have a Gaussian asymptotic behaviour, and cannot directly describe scattering states. This problem is typical of variational calculations, where the basis functions can only reproduce the short-range part of the wave functions. The R-matrix method provides an efficient way to use a finite basis for the determination of scattering properties. In this approach the configuration space is divided in two regions, separated by the channel radius a. In the internal region, the wave function is given by the GCM expansion (1.4.28)

$$\begin{aligned}\Psi_{\rm int}^{\ell m} &= \sum_n f_\ell(R_n)\Phi^{\ell m}(R_n) \\ &= \mathscr{A}\phi_1\phi_2 g_{\rm int}^\ell(\rho)Y_\ell^m(\Omega_\rho).\end{aligned} \tag{1.8.6}$$

The channel radius is chosen large enough to make the nuclear force as well as antisymmetrization between the clusters negligible. Consequently, the external wave function is defined as

$$\Psi_{\rm ext}^{\ell m} = \phi_1\phi_2 g_{\rm ext}^\ell(\rho)Y_\ell^m(\Omega_\rho), \tag{1.8.7}$$

where the radial function $g_{\rm ext}^\ell(\rho)$ is given by (1.8.2).

The quantities to be determined are the collision matrix U_ℓ and the coefficients $f_\ell(R_n)$. The principle of the R-matrix theory is to solve the Schrödinger equation in the internal region, and to use the continuity condition

$$g_{\rm int}^\ell(a) = g_{\rm ext}^\ell(a). \tag{1.8.8}$$

However, as the kinetic-energy operator is not Hermitian over a finite interval, the Schrödinger equation is replaced by the Bloch-Schrödinger equation

$$(H + \mathscr{L} - E)\Psi_{\rm int}^{\ell m} = \mathscr{L}\Psi_{\rm ext}^{\ell m}, \tag{1.8.9}$$

where the Bloch operator [126] acts at $\rho = a$ and is defined as

$$\mathscr{L} = \frac{\hbar^2}{2\mu}\delta(\rho - a)\frac{d}{d\rho}. \tag{1.8.10}$$

Using expansion (1.8.6) in (1.8.9) gives the linear system

$$\sum_{n'} C_{nn'}^\ell f_\ell(R_{n'}) = \langle \Phi^\ell(R_n) \mid \mathscr{L} \mid \Psi_{\rm ext}^\ell \rangle, \tag{1.8.11}$$

where matrix $\mathbf{C}^\ell$ is defined at energy E by

$$C_{nn'}^\ell = \langle \Phi^\ell(R_n)|H + \mathscr{L} - E|\Phi^\ell(R_{n'})\rangle_{\rm int}. \tag{1.8.12}$$

These matrix elements are defined over the internal region. This is achieved by subtracting the external contributions [121]. By definition of the channel radius a, antisymmetrization effects and the nuclear interaction are negligible in the external region. The relevant matrix elements are therefore given by

$$\begin{aligned}
&\langle \Phi^\ell(R_n)|\Phi^\ell(R_{n'})\rangle_{\rm int} = \langle \Phi^\ell(R_n)|\Phi^\ell(R_{n'})\rangle - \int_a^\infty \Gamma_\ell(\rho,R_n)\Gamma_\ell(\rho,R_{n'})\rho^2 d\rho,\\
&\langle \Phi^\ell(R_n)|H|\Phi^\ell(R_{n'})\rangle_{\rm int} = \langle \Phi^\ell(R_n)|H|\Phi^\ell(R_{n'})\rangle\\
&-\int_a^\infty \Gamma_\ell(\rho,R_n)(T_\rho + V_C(\rho) + E_1 + E_2)\Gamma_\ell(\rho,R_{n'})\rho^2 d\rho,
\end{aligned} \tag{1.8.13}$$

where the first terms in the r.h.s. are matrix elements over the whole space, involving Slater determinants. The second terms represent the external contributions of the basis functions and are computed numerically.

From matrix $\mathbf{C}^\ell$, one defines the R matrix

$$R^\ell = \frac{\hbar^2 a}{2\mu}\sum_{nn'}\Gamma_\ell(a,R_n)\left(\mathbf{C}^\ell\right)^{-1}_{nn'}\Gamma_\ell(a,R_{n'}) \tag{1.8.14}$$

which provides the collision matrix as

$$U_\ell = \frac{I_\ell(ka) - kaI'_\ell(ka)R^\ell}{O_\ell(ka) - kaO'_\ell(ka)R^\ell}. \tag{1.8.15}$$

For single-channel calculations the R-matrix and the collision matrix are of dimension one and, strictly speaking, are therefore not matrices. However the tradition is to keep the terminology "matrix", even for single-channel calculations. When the collision matrix is known, coefficients $f_\ell(R_n)$ can be determined from the system (1.8.11). Notice that the channel radius a is not a parameter. In practice, it stems from a compromise: it should be large enough to satisfy the R-matrix conditions, but should be kept as small as possible to limit the number of basis states in the internal region. The stability of the collision matrix and of the wave function with respect to the channel radius is a strong test of the calculation. Further detail concerning the R-matrix method, and its application to microscopic calculations can be found in Refs. [85, 121, 124].

1.9 Applications of the GCM

1.9.1 The 2α and 3α Systems

1.9.1.1 Conditions of the Calculations

The $\alpha+\alpha$ system has been well known for many years, and was one of the first applications of microscopic cluster models. Owing to the large binding energy of the α particle, ^{8}Be is an ideal example of nuclear cluster structure. Two-alpha calculations are rather simple; the matrix elements can be computed from the analytical expressions of Tables 1.3, 1.4 and 1.5. The phase shifts are well known experimentally [127] and can be accurately reproduced by microscopic cluster models associated with the R-matrix method (see, for example, Ref. [128]).

On the other hand, more complicated 3α calculations have also been performed in various three-body models. Here we present a simultaneous study of both systems, as well as a comparison between different 3α descriptions of ^{12}C. The calculations are performed within the same conditions: an oscillator parameter $b=1.36$ fm, and the Minnesota interaction with an admixture parameter $u=0.94687$, as adopted in Ref. [93]. This u value provides a good description of the $\alpha+\alpha$ phase shifts up to 20 MeV, i.e. below the proton threshold. In these conditions, the binding energy of the α particle (independent of u) is $E_\alpha = -24.28$MeV, and the r.m.s. radius is $\sqrt{< r^2 >_\alpha} = \sqrt{9/8}b = 1.44$ fm.

1.9.1.2 The α + α System

The generator coordinates R are taken from 0.8 to 8 fm by step of 0.8 fm. We first present the energy curves, defined as the energy of the system for a fixed generator coordinate R

$$E^\ell(R) = \frac{H_\ell(R,R)}{N_\ell(R,R)}, \tag{1.9.16}$$

and involve the Hamiltonian and overlap kernels.

Using the asymptotic behaviour (1.8.1) of the Hamiltonian provides, at large R values

$$E^\ell(R) \to 2E_\alpha + \frac{\hbar^2}{2\mu}\frac{\ell(\ell+1)}{R^2} + \frac{Z_1Z_2e^2}{R} + \frac{1}{4}\hbar\omega, \tag{1.9.17}$$

where the last contribution comes from a residual kinetic-energy term. The energy curves cannot be considered as nucleus–nucleus potentials, as they do not include forbidden states (see Sect. 1.6). However they provide qualitative properties of the system. In particular the existence of a minimum suggests bound states or resonances, and the location of this minimum provides an estimate of clustering effects.

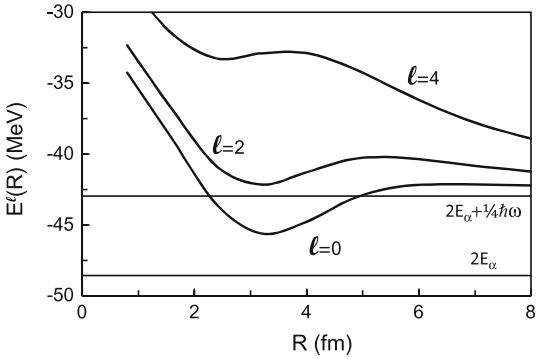

Fig. 1.8 $\alpha + \alpha$ energy curves (1.9.16). Horizontal lines represent threshold energies (see Eq. 1.9.17)

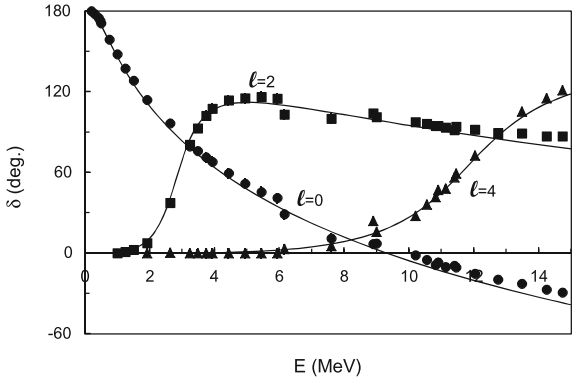

Fig. 1.9 $\alpha + \alpha$ phase shifts for $\ell = 0, 2, 4$. Experimental data are taken from Ref. [127]

The energy curves for $\ell = 0, 2, 4$ are presented in Fig. 1.8. As it is well known, the minimum for $\ell = 0$ is located at fairly large distances ($R \approx 3.2$ fm), which is a strong support for $\alpha + \alpha$ clustering in ^{8}Be. When ℓ increases this minimum moves to smaller distances. It almost disappears for $\ell = 4$, where only a broad resonance can be expected.

The $\alpha + \alpha$ phase shifts are presented in Fig. 1.9 with the experimental data of Ref. [127]. The 0^+ ground state is found at $E = 0.098$ MeV, in fair agreement with experiment ($E = 0.092$ MeV). The broad 2^+ and 4^+ resonances are also well reproduced by the $\alpha + \alpha$ model. Further developments in the $\alpha + \alpha$ system, including monopole distortion of the α particle (i.e. the α wave function is defined by a combination of several b values) can be found, for example, in Refs. [37, 60]. A discussion of the sensitivity to the channel radius is presented in Ref. [124].

1.9.1.3 The 3α System

The ^{12}C nucleus described by a 3α cluster structure has been studied in various microscopic approaches: with a frozen geometry (see, e.g., Refs. [5, 35, 129]), with

an $\alpha + ^8$ Be model [33, 130], and with the hyperspherical formalism [93]. Here we aim at comparing the different approaches within the same conditions. We also complement the hyperspherical calculation presented in Ref. [93].

In multichannel (or multicluster) calculations, the energy curves are defined by a generalization of (1.9.16). For a given generator coordinate R, the Hamiltonian matrix is diagonalized as

$$\sum_j \left(H_{ij}^{J\pi}(R,R) - E^{J\pi}(R) N_{ij}^{J\pi}(R,R) \right) c_j^{J\pi} = 0, \tag{1.9.18}$$

where *i, j* represent the channels (or additional generator coordinates in multicluster problems). We only consider the lowest eigenvalue.

The calculations are performed as follows:

(a) For the frozen geometry, we take an equilateral structure (see Fig. 1.10), with $R_C = 1$–7 fm (by step of 1 fm). A minimum is found near $R_C \approx 2.1$ fm, which is smaller than with the Volkov force [5, 35]. The Volkov force is known to give rise to stronger clustering effects.

(b) For the $\alpha + ^8$Be model (Fig. 1.11), ^{8}Be is described by I=0,2,4 and by 4 generator coordinates $R_2 = 1.4, 2.6, 3.8, 5.0$ fm. These values cover the minima observed in the energy curves (Fig. 1.8). For the $\alpha + ^8$Be motion, we take $R_1 = 1.5$–12.3 fm by step of 1.2 fm. Matrix elements are determined as explained in Ref. [110]. Figure 1.11 displays the $\alpha + ^8$Be energy curves as a function of the generator coordinate R_1. The 0^+ and 2^+ partial waves present a minimum near $R_1 \approx 2$ fm, whereas the 3^- energy curve is typical of a stronger deformation. We illustrate the influence of $\alpha + ^8$Be* excited channels by keeping only the $\alpha + ^8$Be(0^+) configurations (dotted lines). The energy surface (generalization of Eq. (9.18) for two generator coordinates) is presented in Fig. 1.12 for $J = 0^+$. The minimum, corresponding to the ground state of ^{12}C, is obtained for rather small values of R_1 and R_2. At large R_1 values, the dependence on R_2 follows the $\alpha + \alpha$ energy curves of Fig. 1.8.

(c) For the hyperspherical description of the 3α system, we take the generator coordinates R=1.5–15 fm by step of 1.5 fm, and K values up to $K_{\max} = 12$. The energy curves (Fig. 1.13) present a minimum near $R \approx 4$ fm for $J = 0^+, 2^+$ and at larger distance for $J = 3^-$. In Fig. 1.14 we analyze the convergence with respect to $K_{\max}$. This convergence is rather fast, much faster than in non-microscopic models [116].

The ^{12}C energies, obtained by the diagonalization of the full basis, i.e. including all generator coordinates, are shown in Table 1.6 for the $0_1^+, 0_2^+, 2^+$ and 3^- states. Except for the 0_2^+ resonance, the differences between calculations (b) and (c) are of the order of 0.02 MeV, which shows that both bases are equivalent. In contrast, the much simpler model (a) gives a significant underbinding (~ 0.7 MeV). In option (b), considering only I=0 in ^{8}Be provides a non-negligible difference. For the 0_2^+ state which plays a key role in He burning, the $\alpha + ^8$Be description is slightly better than the hyperspherical approach (larger K and R values would be necessary to reach

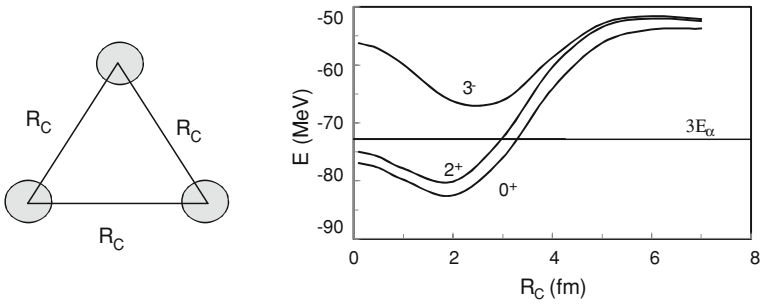

Fig. 1.10 3α structure in model (a) (*left*) and energies (*right*). The α particle is represented by a gray circle

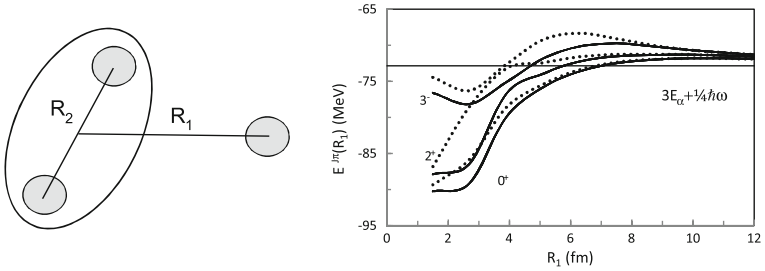

Fig. 1.11 3α structure in model (b) (*left*) and energy curves for different J values (*right*). The dotted lines are obtained with the $\alpha + {}^{8}\mathrm{Be}(0^+)$ channel only

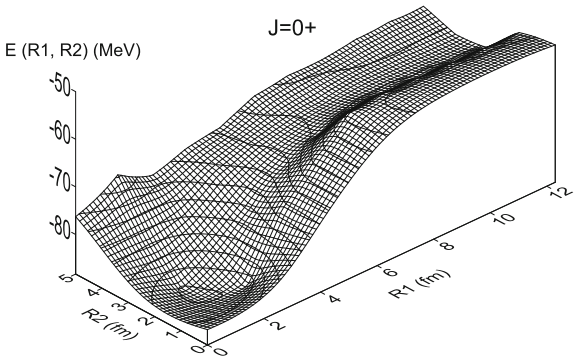

Fig. 1.12 $^{12}\mathrm{C}$ energy surface for $J = 0^+$ as a function of R_1 and R_2

full convergence). For this state the frozen equilateral triangle configuration is not adapted.

In general the 2^+ excitation energy is underestimated. This result is due to the lack of spin–orbit force, whose matrix elements vanish in an α model. Introducing α

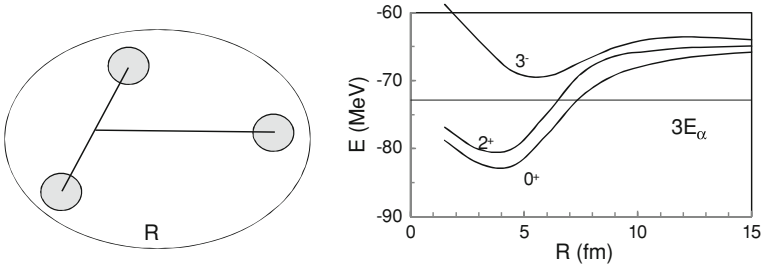

Fig. 1.13 3α structure in hyperspherical model (c) (*left*) and energies (*right*)

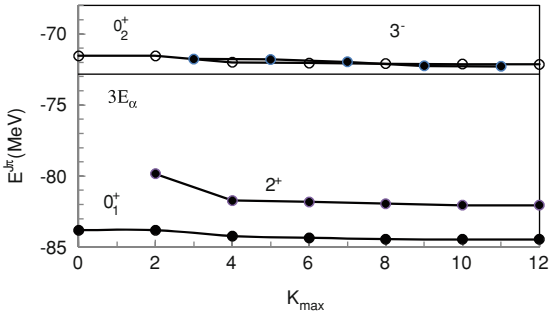

Fig. 1.14 3α binding energies as a function of $K_{\max}$

Table 1.6 Binding energies (in MeV) for various ^{12}C states in models (a), (b) and (c). For model (b), the bracketed values are obtained with $I=0$ only

State	(a)	(b)	(c)
0_1^+	−83.69	−84.44(−84.10)	−84.46
0_2^+	−63.86	−72.23(−72.11)	−72.14
2^+	−81.29	−82.04(−81.41)	−82.06
3^-	−69.03	−72.30(−71.81)	−72.28

breakup configurations increases the 2^+ excitation energy [131], in agreement with experiment. In that case, however, the simplicity of the α cluster model is lost.

1.9.2 Other Applications of the Multicluster Model

In this subsection, we aim to illustrate the multicluster approach with typical results obtained with a five-cluster model [35, 80, 132]. It allows the description of reactions between a nucleus denoted as 1 and a nucleus denoted as 2 and/or to describe spectroscopic properties of the unified nucleus (1 + 2).

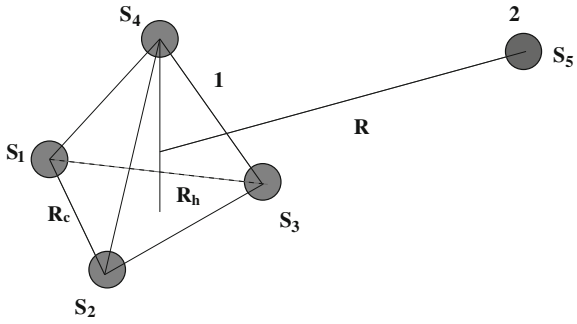

Fig. 1.15 Schematic representation of the five-center model. $\mathbf{S}_i$ are the corresponding vertices

Table 1.7 Binding energies (in MeV) of one-center and four-center wave functions.

	Ground-state	One center	Four centers
^{12}C	0^+	−76.3	−88.0
^{13}C	$1/2^-$	−83.7	−91.7
^{14}C	0^+	−96.1	−103.4
^{15}N	$1/2^-$	−120.7	−126.8
^{16}O	0^+	−140.4	−148.8

A schematic representation is given in Fig. 1.15. Nucleus 1 is described by a tetrahedral structure with three alpha clusters located at the vertices of an equilateral triangle and an additional s-cluster. Typical examples are $^{12}\mathrm{C} = 3\alpha$, $^{13}\mathrm{C} = 3\alpha + n$, and $^{15}\mathrm{N} = 3\alpha + t$. Nucleus 2 is described by a s-cluster and corresponds to an α particle or a nucleon. The set of generator coordinates defining nucleus 1 is defined as $R_{\{C\}} = (R_c, R_h)$ (see Fig. 1.15).

To test the cluster description of nucleus 1, we first analyze properties of some p-shell nuclei described by a tetrahedral structure [35]. The calculations with the four-cluster model are performed with a mixing of (R_c, R_h) configurations, whereas one-center results are obtained with $R_c = R_h = 0$. The oscillator parameter is optimized to minimize the binding energy. The nucleon–nucleon interaction is the Volkov force V2 (with the standard value M=0.6), and the spin–orbit amplitude is chosen as $S_0 = 30\,\mathrm{MeV.fm}^5$. The spin–orbit force does not contribute to ^{12}C, ^{14}C and ^{16}O since the clusters have an intrinsic spin zero.

Table 1.7 compares the ground-state binding energies in a one-center model and in a four-centers model. The binding energies obtained within the four-center model are always lower with a quite substantial difference.

Table 1.8 shows typical $E2$ transition probabilities and the ^{12}C quadrupole moment. Clearly the introduction of clustering effects in these nuclei improve the wave functions. The four-cluster results are in good agreement with experiment, whereas the no-cluster approximation underestimates the $E2$ properties.

We illustrate five-cluster calculations with the $\alpha+^{16}$O system, described by five α clusters [80]. It is well-known that several ^{20}Ne states present a marked $\alpha+^{16}$O

Table 1.8 ^{12}C quadrupole moment (in $e.\text{fm}^2$) and reduced transition probabilities (in W.u.). Experimental data are taken from Refs. [133, 134].

		One-center	Four-center	Experiment
^{12}C	$Q(2^+)$	3.0	5.4	6 ± 3
	$B(E2, 2^+ \to 0^+)$	2.0	4.5	4.65 ± 0.26
^{13}C	$B(E2, 3/2^- \to 1/2^-)$	1.5	3.4	3.5 ± 0.8
	$B(E2, 5/2^- \to 1/2^-)$	1.0	3.1	3.1 ± 0.2

Table 1.9 α-width (in keV) of some ^{20}Ne states in the $K = 0^-$ band. Experimental data are taken from Ref. [135]

J^π	Two centers	Five centers (0^+)	Five-centers (0^+, 3^-, 1^-)	Experiment
1^-	0.042	0.032	0.031	0.028 ± 0.003
3^-	13.0	10.8	10.6	8.2 ± 0.3
5^-	200	173	169	145 ± 40
7^-	700	570	530	310 ± 30

structure. The ^{20}Ne nucleus is described by $\alpha + {}^{16}$O channels where the 0^+ ground state and the 1^- and 3^- excited states are considered. For computer-time reasons, only one set of generator coordinates ($R_c = 1.8\,\text{fm}, R_h = 2.5\,\text{fm}$) is selected to describe the ^{16}O nucleus. These values minimize the ^{16}O binding energy.

We focus here on α widths of some states in the $K = 0^-$ band. They are obtained within the R-matrix formalism. Results are gathered in Table 1.9 and obtained in three different ways: the standard two-cluster model where ^{16}O is described by a closed p-shell structure, the multicluster approach with only the ^{16}O ground state, and with some excited channels. The α widths are overestimated in the two-center approach, but are significantly reduced when clustering effects are included in ^{16}O. Excited channels still improve the comparison with experiment.

In Ref. [80] the spectroscopy of ^{20}Ne was complemented by calculations of the $\alpha + {}^{16}$O phase shifts and of the $^{16}\text{O}(\alpha, \gamma)^{20}\text{Ne}$ radiative-capture cross section. As mentioned in Sect. 1.8, the cluster model can be extended to scattering states with the R-matrix method, which provides scattering properties (such as resonance widths) and cross sections.

1.9.3 Multichannel Study of the $^{17}F(p, \gamma)^{18}Ne$ Reaction

The knowledge of the $^{17}\text{F}(\text{p}, \gamma)^{18}\text{Ne}$ reaction rate is important for the understanding of novae and X-ray bursts [136]. The energy range characteristic of such astrophysical events can be evaluated by the calculation of the Gamow energy E_G and the width of the Gamow peak Δ_0 [137]. For a typical temperature T=0.5 GK, these values

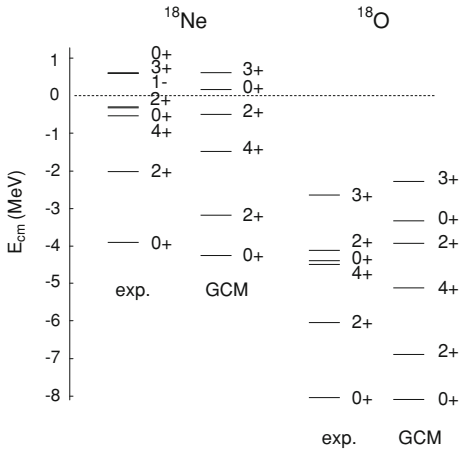

Fig. 1.16 ^{18}Ne and ^{18}O energy spectra (taken from Ref. [136]) with respect to the nucleon threshold (*dotted line*)

are $E_G = 0.32\,\text{MeV}$ and $\Delta_0 = 0.28\,\text{MeV}$. Until now, a direct measurement of the $^{17}\text{F(p, }\gamma)^{18}\text{Ne}$ cross section down to these energies has not been performed.

It is now well established that the $3^+_1(\ell = 0)$ resonance at $E_{cm} = 0.64\,\text{MeV}$ dominates the $^{17}\text{F(p, }\gamma)^{18}\text{Ne}$ reaction rate at stellar temperatures. The energy and the proton width have been measured by Bardayan et al. [138]. However, the gamma width which determines the reaction rate is experimentally unknown and is estimated from theoretical calculations.

The predictive power of the GCM is of particular interest in such a context. Indeed, the small number of parameters allows reliable calculations in the astrophysical energy range. The ^{18}Ne wave functions are defined as a combination of $^{17}\text{F} + \text{p}$ and $^{14}\text{O} + \alpha$ channel functions. The ^{17}F internal wave functions are defined from all possible Slater determinants with one proton in the *sd* shell, the *s* and *p* shells being filled. This provides the well known shell-model states with spin $I_1 = 5/2^+, 1/2^+$, and $3/2^+$. Similarly, the ^{14}O internal wave functions are defined from four neutrons in the *p* shell, the *s* shell being filled for the neutron part, and the *s* and *p* shells being filled for the proton part. This provides two states with $I_1 = 0^+$, one state with $I_1 = 1^+$ and two states with $I_1 = 2^+$ (see Sect. 7.2). The nucleon–nucleon interaction is fitted to the 3^+ energy. Further detail about the conditions of the calculation is given in Ref. [136].

The ^{18}Ne spectrum is shown in Fig. 1.16 along with the ^{18}O mirror nucleus. We find a good overall agreement with experiment. The state ordering below the $^{17}\text{F} + \text{p}$ threshold is well reproduced, except for the 0^+_2 state, slightly unbound in the GCM. However the difference with the experimental value is only of 0.49 MeV. We can also notice the good description of the 2^+_2 state.

The important 3^+_1 resonance is known to have a single-particle structure, and is well described in a $^{17}\text{F} + \text{p}$ model. The energy is adjusted by the nucleon–nucleon force, but the proton width $\Gamma_p = 21.1\,\text{keV}$ is obtained without any fitting procedure. The GCM value is in very good agreement with experiment ($\Gamma_p = 18.0 \pm 2_{\text{stat}} \pm$

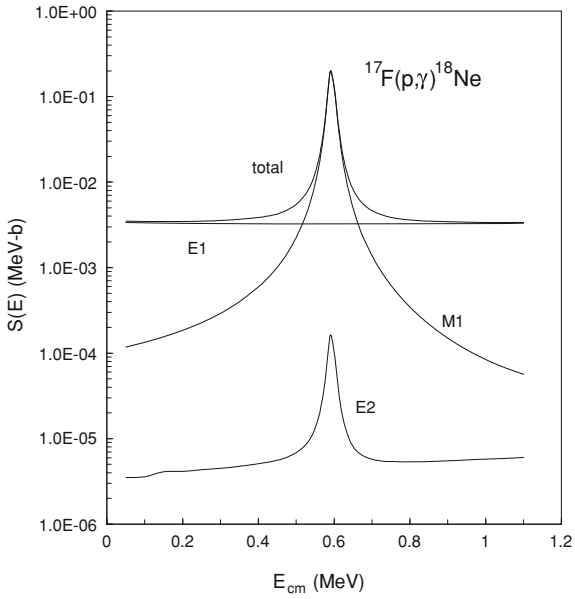

Fig. 1.17 ^{17}F(p, γ)^{18}Ne astrophysical S-factor with the contribution of different multipolarities (taken from Ref. [136])

$1_{\rm sys}$ keV). The predicted gamma width $\Gamma_\gamma = 33$ meV is similar to values deduced from the shell model, and used in astrophysics ($\Gamma_\gamma = 30 \pm 20$ meV) [138].

The total and partial S-factors are displayed in Fig. 1.17. The astrophysical S-factor is related to the cross section $\sigma(E)$ as

$$S(E) = E\sigma(E)\exp(2\pi\eta), \tag{1.9.19}$$

where η is the Sommerfeld parameter defined in Sect. 1.8.2. The calculations are performed for the $E1$, $E2$, and $M1$ multipolarities, and the 0_1^+, 2_1^+, 2_2^+ and 4_1^+ bound states are considered. As expected, the non-resonant $E1$ transitions give the dominant contribution below the 3_1^+ state. At zero energy, the S-factor is entirely determined by the $E1$ term. The calculation gives $S(0) = 3.5$ keV-b. On the contrary, the $M1$ contribution is dominant near the resonance (the $E2$ term is negligible). More detailed calculations [136] show that transitions to the 2_1^+ and 2_2^+ bound states represent the main parts of the S-factor.

The ^{17}F(p, γ)^{18}Ne reaction rate is usually calculated as a sum of a direct component and of a resonant term taking into account the 1_1^-, 3_1^+ and 0_3^+ contributions in ^{18}Ne [139]. One of the main advantages of our method is to perform calculations without separation between resonant and non-resonant contributions. However, in the present case our model is unable to reproduce the 1_1^- and 0_3^+ low-energy resonances. Their contribution to the rate can be treated separately taking energies and total widths from experiment [139].

All these results illustrate the adequacy and limitations of the present framework for reactions of astrophysical interest. Here, two states located in the astrophysical

energy range are not reproduced by the GCM: the 1^-_1 and 0^+_3 states. This means that the multichannel basis is not sufficient, and that other configurations should be introduced. Owing to the fact that the main contribution comes here from the 3^+_1 resonance, this problem is however minor.

Another drawback comes from the lack of degrees of freedom in the Volkov interaction. The present parameter choice leads to a strong overestimate of the $(^{14}\mathrm{O}+\alpha)-(^{17}\mathrm{F}+\mathrm{p})$ threshold: 15.43 MeV to be compared with the experimental value 1.19 MeV [140]. This can be explained by the fact that the model gives a better description of ^{17}F than of ^{14}O. This problem prevents the simultaneous study of the $^{14}\mathrm{O}(\alpha,\mathrm{p})^{17}\mathrm{F}$ transfer reaction. For these reasons, we have developed the EVI [141] (see Sect. 1.2 for more detail), a new interaction with an additional parameter which allows to fit two important properties of the system such as a resonance energy and a threshold value. This interaction is well suited to transfer reactions where the reproduction of the Q value is crucial. Applications in nuclear astrophysics can be found, for example, in Ref. [142].

1.9.4 ^{12}Be as an Example of a Light Exotic Nucleus

Due to technical difficulties, experimental informations related to the study of exotic light nuclei are in general limited. From a theoretical point of view, cluster models appear to be particularly well adapted to study such nuclei. In particular, the exact treatment of the asymptotic behavior of the wave functions through the MRM (see Sect. 1.8) allows the description of unbound states. A cluster model is also well suited to molecular states, which present a strong deformation.

We illustrate applications of the GCM with a recent study performed on the ^{12}Be nucleus [14], by focusing on molecular states. Above the ^{6}He+^{6}He threshold, 4^+, 6^+ and 8^+ states have been identified in the breakup of ^{12}Be into the ^{6}He+^{6}He and $^8\mathrm{He}+\alpha$ channels by Freer et al. [143]. They are believed to be members of a molecular band.

A multi-channel wave function is given by a superposition of $^8\mathrm{He}+\alpha$ and ^{6}He+^{6}He components. The 0^+ internal wave functions of ^{6}He and ^{8}He are built in a one-center harmonic oscillator model with $(p_{3/2})^2$ and $(p_{3/2})^4$ configurations, respectively and the 2^+ states, with $(p_{3/2})(p_{1/2})$ and $(p_{3/2})^3(p_{1/2})^1$ configurations, respectively. Details on the conditions of the calculations are given in Ref. [14]. The present calculation updates an earlier study [13], where only ground-state configurations were included.

The calculation (see Fig. 1.18) supports the existence of a molecular band, as proposed by Freer et al. [143] and by Saito et al. [144]. The large reduced widths support the molecular structure of this band. The analysis of the dimensionless reduced widths shows that the 0^+ wave function is dominated by the $^6\mathrm{He}(0^+)+{}^6\mathrm{He}(0^+)$ channel. The theoretical 2^+ and 4^+ energies are in good agreement with the results of Saito et al. [144] and of Freer et al. [143], respectively.

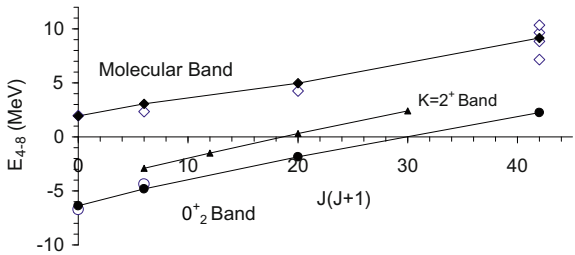

Fig. 1.18 Positive-parity ^{12}Be states predicted by the GCM (full symbols) and experimental candidates (open symbols [143–145])

The wave functions are dominated by the $^{6}\mathrm{He}(0^{+}) + ^{6}\mathrm{He}(0^{+})$ and $^{8}\mathrm{He}(0^{+}) + \alpha$ ground-state configurations.

The 0_2^+ and 2_2^+ states are well reproduced by the GCM. Indeed, the energy difference with experiment is less than 0.5 MeV for both states (see Fig. 1.18). According to Refs. [146–148], we confirm that these states belong to a same 0_2^+ band and we propose other band members. The calculation shows that the wave functions of the 0_2^+-band members are dominated by the $^{8}\mathrm{He} + \alpha$ channels.

With this example, we have illustrated the ability of the GCM to describe molecular states. Indeed, we have reproduced many known states of ^{12}Be, in particular those belonging to a molecular band. We have also predicted new ^{12}Be bands which could be searched for in future experimental studies.

1.10 Conclusions

In this work, we have reviewed various aspects of microscopic cluster models. With respect to non-microscopic variants, microscopic theories offer several advantages: in particular, they only depend on a nucleon–nucleon interaction, and excited configurations can be introduced without further parameters. The cluster approximation makes them tractable, even for fairly large nucleon numbers. Of course, cluster models use effective interactions.

Microscopic cluster models are applied in many topics; using the microscopic R-matrix method, they can be consistently extended to scattering states [124]. This property opens many perspectives in low-energy nuclear physics. Not only cross sections can be studied, but spectroscopic applications can be extended to unbound states, even with a broad width [149]. The microscopic treatment of two-cluster scattering states is well known, but this formalism has been recently extended to three-cluster scattering states [95].

We have illustrated the formalism with some typical examples, both in spectroscopy and in reactions. In the literature, the GCM has been applied to many fields, ranging from the spectroscopy of exotic nuclei to reactions of astrophysical interest. Microscopic cluster models represent a efficient tool for the investigation of nuclei located near or beyond the driplines. These nuclei, such as ^{16}B or ^{18}B

for example [150], are now actively studied in large-scale facilities. They combine several difficulties: they are unbound even in their ground state, excited states of the core are expected to be important, and core-neutron interactions (such as ^{15}B + n or ^{17} B+n) are not available. Investigations of Bose–Einstein condensation [8] in nuclear physics also benefit from cluster models. In the future, scattering theories could be developed with microscopic cluster wave functions of the projectile, in particular for the Continuum Discretized Coupled Channel (CDCC) method [99], or for the eikonal method [151]. The merging of precise scattering models with microscopic descriptions of the projectile represents a challenge for the upcoming years.

Acknowledgments This text presents research results of the IAP program P6/23 initiated by the Belgian-state Federal Services for Scientific, Technical and Cultural Affairs.

References

1. Brink, D.M.: J. Phys. Conf. Ser. **111**, 012001 (2008)
2. Wheeler, J.A.: Phys. Rev. **52**, 1083 (1937)
3. Margenau, H.: Phys. Rev. **59**, 3 (1941)
4. Brink, D.: Proc. Int. School "Enrico Fermi" 36, Varenna 1965, p. 247. Academic Press, New-York (1966)
5. Fujiwara, Y., Horiuchi, H., Ikeda, K., Kamimura, M., Katō, K., Suzuki, Y., Uegaki, E.: Prog. Theor. Phys. Suppl. **68**, 29 (1980)
6. Hoyle, F.: Astrophys. J. Suppl. **1**, 121 (1954)
7. Ikeda, K., Takigawa, N., Horiuchi, H.: Prog. Theor. Phys. Suppl., Extra Number p. 464 (1968)
8. Tohsaki, A., Horiuchi, H., Schuck, P., Röpke, G.: Phys. Rev. Lett. **87**, 192501 (2001)
9. von Oertzen, W., Freer, M., Kanada-En'yo, Y.: Phys. Rep. **432**, 43 (2006)
10. Freer, M.: Rep. Prog. Phys. **70**, 2149 (2007)
11. Fujiwara, Y., Tang, Y.C.: Phys. Rev. C **31**, 342 (1985)
12. Freer, M., Angélique, J.C., Axelsson, L., Benoit, B., Bergmann, U., Catford, W.N., Chappell, S.P.G., Clarke, N.M., Curtis, N., D'Arrigo, A., DeGóes Brennand, E., Dorvaux, O., Fulton, B.R., Giardina, G., Gregori, C., Grevy, S., Hanappe, F., Kelly, G., Labiche, M., Brun, C.L., Leenhardt, S., Lewitowicz, M., Markenroth, K., Marqués, F.M., Motta, M., Murgatroyd, J.T., Nilsson, T., Ninane, A., Orr, N.A., Piqueras, I., Laurent, M.G.S., Singer, S.M., Sorlin, O., Stuttgé, L., Watson, D.L.: Phys. Rev. Lett. **82**, 1383 (1999)
13. Descouvemont, P., Baye, D.: Phys. Lett. **505B**, 71 (2001)
14. Dufour, M., Descouvemont, P., Nowacki, F.: Nucl. Phys. A **836**, 242 (2010)
15. Wildermuth, K., Kanellopoulos, T.: Nucl. Phys. **9**, 449 (1958)
16. Tang, Y.C.: in Topics in Nuclear Physics II Lecture Notes in Physics. Vol. 145, p. 572 Springer, Berlin (1981)
17. Johnson, E.D., Rogachev, G.V., Goldberg, V.Z., Brown, S., Robson, D., Crisp, A.M., Cottle, P.D., Fu, C., Giles, J., Green, B.W., Kemper, K.W., Lee, K., Roede, B.T., Tribble, R.E.: Eur. Phys. J. A **42**, 135 (2009)
18. Neudatchin, V.G., Kukulin, V.I., Korotkikh, V.L., Korennoy, V.P.: Phys. Lett. **34B**, 581 (1971)
19. Buck, B., Dover, C.B., Vary, J.P.: Phys. Rev. C **11**, 1803 (1975)
20. Wildermuth, K., Tang, Y.C.: A Unified Theory of the Nucleus. Vieweg, Braunschweig (1977)
21. Suzuki, Y., Varga, K.: Stochastic variational approach to quantum-mechanical few-body problems. Lecture Notes in Physics Vol. m54 (1998)
22. Baye, D.: Phys. Rev. Lett. **58**, 2738 (1987)
23. Lin, C.D.: Phys. Rep. **257**, 1 (1995)

24. Faddeev, L., Merkuriev, S.: Quantum Scattering Theory for Several Particle Systems. Kluwer Academic Publishers, Dordrecht (1993)
25. Tohsaki, A.: Phys. Rev. C **49**, 1814 (1994)
26. Caurier, E., Martínez-Pinedo, G., Nowacki, F., Poves, A., Zuker, A.P.: Rev. Mod. Phys. **77**, 427 (2005)
27. Navrátil, P., Vary, J.P., Barrett, B.R.: Phys. Rev. Lett. **84**, 5728 (2000)
28. Kanada-En'yo, Y., Horiuchi, H., Ono, A.: Phys. Rev. C **52**, 628 (1995)
29. Neff, T., Feldmeier, H.: Eur. Phys. J. Spec. Top. **156**, 69 (2008)
30. Kievsky, A., Rosati, S., Viviani, M., Marcucci, L.E., Girlanda, L.: J. Phys. G **35**, 063101 (2008)
31. Saito, S.: Prog. Theor. Phys. Suppl. **62**, 11 (1977)
32. Horiuchi, H.: Prog. Theor. Phys. Suppl. **62**, 90 (1977)
33. Kamimura, M.: Nucl. Phys. A **351**, 456 (1981)
34. Varga, K., Suzuki, Y., Tanihata, I.: Phys. Rev. C **52**, 3013 (1995)
35. Dufour, M., Descouvemont, P.: Nucl. Phys. A **605**, 160 (1996)
36. Descouvemont, P.: Nucl. Phys. A **596**, 285 (1996)
37. Baye, D., Kruglanski, M.: Phys. Rev. C **45**, 1321 (1992)
38. Descouvemont, P., Baye, D.: Phys. Lett. B **169**, 143 (1986)
39. Wada, T., Horiuchi, H.: Phys. Rev. C **38**, 2063 (1988)
40. Dufour, M., Descouvemont, P.: Nucl. Phys. A **726**, 53 (2003)
41. Tanihata, I., Hamagaki, H., Hashimoto, O., Shida, Y., Yoshikawa, N., Sugimoto, K., Yamakawa, O., Kobayashi, T., Takahashi, N.: Phys. Rev. Lett. **55**, 2676 (1985)
42. Jonson, B.: Phys. Rep. **389**, 1 (2004)
43. Varga, K., Suzuki, Y., Ohbayasi, Y.: Phys. Rev. C **50**, 189 (1994)
44. Descouvemont, P.: Nucl. Phys. A **584**, 532 (1995)
45. Korennov, S., Descouvemont, P.: Nucl. Phys. A **740**, 249 (2004)
46. Adahchour, A., Descouvemont, P.: Nucl. Phys. A **813**, 252 (2008)
47. Baye, D., Descouvemont, P.: Phys. Rev. C **38**, 2463 (1988)
48. Tursunov, E.M., Baye, D., Descouvemont, P.: Phys. Rev. C **73**, 014303 (2006)
49. Liu, Q.K.K., Kanada, H., Tang, Y.C.: Phys. Rev. C **23**, 645 (1981)
50. Dufour, M., Descouvemont, P.: Phys. Rev. C **78**, 015808 (2008)
51. Langanke, K.: Adv. Nucl. Phys. **21**, 85 (1994)
52. Descouvemont, P.: Phys. Rev. C **70**, 065802 (2004)
53. Iliadis, C.: Nuclear Physics of Stars. Wiley, Weinheim (2007)
54. Baye, D., Descouvemont, P., Kruglanski, M.: Nucl. Phys. A **550**, 250 (1992)
55. Tang, Y.C., LeMere, M., Thompsom, D.R.: Phys. Rep. **47**, 167 (1978)
56. Wildermuth, K., Kanellopoulos, E.J.: Rep. Prog. Phys. **42**, 1719 (1979)
57. Friedrich, H.: Phys. Rep. **74C**, 209 (1981)
58. Bertsch, G., Borysowicz, J., Mcmanus, H., Love, W.G.: Nucl. Phys. A **284**, 399 (1977)
59. Volkov, A.B.: Nucl. Phys. **74**, 33 (1965)
60. Thompson, D.R., LeMere, M., Tang, Y.C.: Nucl. Phys. A **286**, 53 (1977)
61. Baye, D., Pecher, N.: Bull. Cl. Sci. Acad. Roy. Belg. **67**, 835 (1981)
62. Navrátil, P., Quaglioni, S., Stetcu, I., Barrett, B.R.: J. Phys. G **36**, 083101 (2009)
63. Navrátil, P., Kamuntavičius, G.P., Barrett, B.R.: Phys. Rev. C **61**, 044001 (2000)
64. Wiringa, R.B., Stoks, V.G.J., Schiavilla, R.: Phys. Rev. C **51**, 38 (1995)
65. Machleidt, R.: Phys. Rev. C **63**, 024001 (2001)
66. Navrátil, P., Gueorguiev, V.G., Vary, J.P., Ormand, W.E., Nogga, A.: Phys. Rev. Lett. **99**, 042501 (2007)
67. Tohsaki-Suzuki, A.: Prog. Theor. Phys. Suppl. **62**, 191 (1977)
68. Quaglioni, S., Navrátil, P.: Phys. Rev. C **79**, 044606 (2009)
69. Hesse, M., Sparenberg, J.M., Van Raemdonck, F., Baye, D.: Nucl. Phys. A **640**, 37 (1998)
70. Thompson, D.R., Tang, Y.C.: Phys. Rev. C **4**, 306 (1971)
71. Theeten, M., Baye, D., Descouvemont, P.: Phys. Rev. C **74**, 044304 (2006)

72. Suzuki, Y.: Nucl. Phys. A **405**, 40 (1983)
73. J. Raynal, Computing as a language of physics, Trieste 1971, p. 281. IAEA, Vienna (1972)
74. Baye, D.: Phys. Stat. Sol. (b) **243**, 1095 (2006)
75. Horiuchi, H.: Prog. Theor. Phys. **43**, 375 (1970)
76. Timofeyuk, N.K., Descouvemont, P.: Phys. Rev. C **71**, 064305 (2005)
77. Dufour, M., Descouvemont, P.: Nucl. Phys. A **785**, 381 (2007)
78. Lawson, R.D.: Theory of The Nuclear Shell Model. Clarendon, Oxford (1980)
79. Bethe, H.A., Rose, M.E.: Phys. Rev. **51**, 283 (1937)
80. Dufour, M., Descouvemont, P., Baye, D.: Phys. Rev. C **50**, 795 (1994)
81. Aoki, K., Horiuchi, H.: Prog. Theor. Phys. **68**, 2028 (1982)
82. Descouvemont, P., Baye, D.: Nucl. Phys. A **517**, 143 (1990)
83. Gartenhaus, S., Schwartz, C.: Phys. Rev. **108**, 482 (1957)
84. Rose, H.J., Brink, D.M.: Rev. Mod. Phys. **39**, 306 (1967)
85. Baye, D., Descouvemont, P.: Nucl. Phys. A **407**, 77 (1983)
86. Tohsaki-Suzuki, A.: Prog. Theor. Phys. **59**, 1261 (1978)
87. Hill, D.L., Wheeler, J.A.: Phys. Rev. **89**, 1102 (1953)
88. Friedrich, H.: Nucl. Phys. A **224**, 537 (1974)
89. Abramowitz, M., Stegun, I.A.: Handbook of Mathematical Functions. Dover, London (1972)
90. Baye, D., Salmon, Y.: Nucl. Phys. A **331**, 254 (1979)
91. Varga, K., Lovas, R.G.: Phys. Rev. C **37**, 2906 (1988)
92. Saito, S.: Prog. Theor. Phys. **41**, 705 (1969)
93. Suzuki, Y., Matsumura, H., Orabi, M., Fujiwara, Y., Descouvemont, P., Theeten, M., Baye, D.: Phys. Lett. B **659**, 160 (2008)
94. Baye, D., Descouvemont, P.: Ann. Phys. **165**, 115 (1985)
95. Damman, A., Descouvemont, P.: Phys. Rev. C **80**, 044310 (2009)
96. Theeten, M., Matsumura, H., Orabi, M., Baye, D., Descouvemont, P., Fujiwara, Y., Suzuki, Y.: Phys. Rev. C **76**, 054003 (2007)
97. Fujiwara, Y., Suzuki, Y., Miyagawa, K., Kohno, M., Nemura, H.: Prog. Theor. Phys. **107**, 993 (2002)
98. Descouvemont, P., Tursunov, E.M., Baye, D.: Nucl. Phys. A **765**, 370 (2006)
99. Austern, N., Iseri, Y., Kamimura, M., Kawai, M., Rawitscher, G., Yahiro, M.: Phys. Rep. **154**, 125 (1987)
100. Fujiwara, Y., Suzuki, Y., Kohno, M., Miyagawa, K.: Phys. Rev. C **77**, 027001 (2008)
101. Kanada, H., Kaneko, T., Nagata, S., Nomoto, M.: Prog. Theor. Phys. **61**, 1327 (1979)
102. Buck, B., Friedrich, H., Wheatley, C.: Nucl. Phys. A **275**, 246 (1977)
103. Hutson, J.M.: Comput. Phys. Commun. **84**, 1 (1994)
104. Buck, B., Baldock, R.A., Rubio, J.A.: J. Phys. G **11**, L11 (1985)
105. Descouvemont, P.: Nucl. Phys. A **655**, 440 (1999)
106. Descouvemont, P.: Astrophys. J. **543**, 425 (2000)
107. Messiah, A.: Quantum Mechanics. Dover Publications, New York (1999)
108. Descouvemont, P.: Phys. Rev. C **47**, 210 (1993)
109. Descouvemont, P.: Nucl. Phys. A **615**, 261 (1997)
110. Descouvemont, P., Baye, D.: Nucl. Phys. A **463**, 629 (1987)
111. Descouvemont, P., Baye, D.: Nucl. Phys. A **573**, 28 (1994)
112. Baye, D., Suzuki, Y., Descouvemont, P.: Prog. Theor. Phys. **91**, 271 (1994)
113. Descouvemont, P.: Phys. Rev. C **44**, 306 (1991)
114. Zhukov, M.V., Danilin, B.V., Fedorov, D.V., Bang, J.M., Thompson, I.J., Vaagen, J.S.: Phys. Rep. **231**, 151 (1993)
115. Raynal, J., Revai, J.: Nuovo Cim. A **39**, 612 (1970)
116. Descouvemont, P., Daniel, C., Baye, D.: Phys. Rev. C **67**, 044309 (2003)
117. Thompson, I.J., Danilin, B.V., Efros, V.D., Vaagen, J.S., Bang, J.M., Zhukov, M.V.: Phys. Rev. C **61**, 024318 (2000)
118. Adahchour, A., Descouvemont, P.: J. Phys. G **37**, 045102 (2010)

119. Lane, A.M., Thomas, R.G.: Rev. Mod. Phys. **30**, 257 (1958)
120. Thompson, I.J.: Comput. Phys. Rep. **7**, 167 (1988)
121. Baye, D., Heenen, P.-H., Libert-Heinemann, M.: Nucl. Phys. A **291**, 230 (1977)
122. Hesse, M., Roland, J., Baye, D.: Nucl. Phys. A **709**, 184 (2002)
123. Quaglioni, S., Navrátil, P.: Phys. Rev. Lett. **101**, 092501 (2008)
124. Descouvemont, P., Baye, D.: Rep. Prog. Phys. **73**, 036301 (2010)
125. Descouvemont, P.: Theoretical Models for Nuclear Astrophysics. Nova Science, New York (2003)
126. Bloch, C.: Nucl. Phys. **4**, 503 (1957)
127. Afzal, S.A., Ahmad, A.A.Z., Ali, S.: Rev. Mod. Phys. **41**, 247 (1969)
128. Baye, D., Heenen, P.-H.: Nucl. Phys. A **233**, 304 (1974)
129. Uegaki, E., Okabe, S., Abe, Y., Tanaka, H.: Prog. Theor. Phys. **57**, 1262 (1977)
130. Descouvemont, P., Baye, D.: Phys. Rev. C **36**, 54 (1987)
131. Itagaki, N., Aoyama, S., Okabe, S., Ikeda, K.: Phys. Rev. C **70**, 054307 (2004)
132. Dufour, M., Descouvemont, P.: Phys. Rev. C **56**, 1831 (1997)
133. Ajzenberg-Selove, F.: Nucl. Phys. A **506**, 1 (1990)
134. Ajzenberg-Selove, F.: Nucl. Phys. A **523**, 1 (1991)
135. Ajzenberg-Selove, F.: Nucl. Phys. A **475**, 1 (1987)
136. Dufour, M., Descouvemont, P.: Nucl. Phys. A **730**, 316 (2004)
137. Clayton, D.D.: Principles of Stellar Evolution and Nucleosynthesis. The University of Chicago Press, Chicago (1983)
138. Bardayan, D.W., Blackmon, J.C., Brune, C.R., Champagne, A.E., Chen, A.A., Cox, J.M., Davinson, T., Hansper, V.Y., Hofstee, M.A., Johnson, B.A., Kozub, R.L., Ma, Z., Parker, P.D., Pierce, D.E., Rabban, M.T., Shotter, A.C., Smith, M.S., Swartz, K.B., Visser, D.W., Woods, P.J.: Phys. Rev. C **62**, 055804 (2000)
139. García, A., Adelberger, E.G., Magnus, P.V., Markoff, D.M., Swartz, K.B., Smith, M.S., Hahn, K.I., Bateman, N., Parker, P.D.: Phys. Rev. C **43**, 2012 (1991)
140. Tilley, D.R., Weller, H.R., Cheves, C.M., Chasteler, R.M.: Nucl. Phys. A **595**, 1 (1995)
141. Dufour, M., Descouvemont, P.: Nucl. Phys. A **750**, 218 (2005)
142. Dufour, M., Descouvemont, P.: Phys. Rev. C **72**, 015801 (2005)
143. Freer, M., Angélique, J.C., Axelsson, L., Benoit, B., Bergmann, U., Catford, W.N., Chappell, S.P.G., Clarke, N.M., Curtis, N., D'Arrigo, A., DeGóes Brennand, E., Dorvaux, O., Fulton, B.R., Giardina, G., Gregori, C., Grevy, S., Hanappe, F., Kelly, G., Labiche, M., Le Brun, C., Leenhardt, S., Lewitowicz, M., Markenroth, K., Marqués, F.M., Murgatroyd, J.T., Nilsson, T., Ninane, A., Orr, N.A., Piqueras, I., Laurent, M.G.S., Singer, S.M., Sorlin, O., Stuttgé, L., Watson, D.L.: Phys. Rev. C **63**, 034301 (2001)
144. Saito, A., Shimoura, S., Takeuchi, S., Motobayashi, T., Minemura, T., Matsuyama, Y., Baba, H., Akiyoshi, H., Ando, Y., Aoi, N., Fülöp, Z., Gomi, T., Higurashi, Y., Hirai, M., Ieki, K., Imai, N., Iwasa, N., Iwasaki, H., Iwata, Y., Kanno, S., Kobayashi, H., Kubono, S., Kunibu, M., Kurokawa, M., Liu, Z., Michimasa, S., Nakamura, T., Ozawa, S., Sakurai, H., Serata, M., Takeshita, E., Teranishi, T., Ue, K., Yamada, K., Yanagisawa, Y., Ishihara, M.: Nucl. Phys. A **738**, 337 (2004)
145. Shimoura, S., Ota, S., Demichi, K., Aoi, N., Baba, H., Elekes, Z., Fukuchi, T., Gomi, T., Hasegawa, K., Ideguchi, E., Ishihara, M., Iwasa, N., Iwasaki, H., Kanno, S., Kubono, S., Kurita, K., Kurokawa, M., Matsuyama, Y., Michimasa, S., Miller, K., Minemura, T., Motobayashi, T., Murakami, T., Notani, M., Odahara, A., Saito, A., Sakurai, H., Takeshita, E., Takeuchi, S., Tamaki, M., Teranishi, T., Yamada, K., Yanagisawa, Y., Hamamoto, I.: Phys. Lett. B **654**, 87 (2007)
146. Kanada-En'yo, Y., Horiuchi, H.: Phys. Rev. C **68**, 014319 (2003)
147. Ito, M., Itagaki, N., Sakurai, H., Ikeda, K.: Phys. Rev. Lett. **100**, 182502 (2008)
148. Bohlen, H.G., von Oertzen, W., Kokalova, T., Schulz, C., Kalpakchieva, R., Massey, T.N., Milin, M.: Int. J. Mod. Phys. E **17**, 2067 (2008)
149. Baye, D., Descouvemont, P., Leo, F.: Phys. Rev. C **72**, 024309 (2005)

150. Lecouey, J.L., Orr, N., Marqués, F., Achouri, N., Angélique, J.C., Brown, B., Carstoiu, F., Catford, W., Clarke, N., Freer, M., Fulton, B., Grévy, S., Hanappe, F., Jones, K., Labiche, M., Lemmon, R., Ninane, A., Sauvan, E., Spohr, K., Stuttgé, L.: Phys. Lett. B **672**, 6 (2009)
151. Suzuki, Y., Lovas, R.G., Yabana, K., Varga, K.: Structure and Reactions of Light Exotic Nuclei. Taylor & Francis, London (2003)